Article (refereed) - postprint

Guallart, Elisa F.; Schuster, Ute; Fajar, Noelia M.; Legge, Oliver; Brown, Peter; Pelejero, Carles; Messias, Marie-Jose; Calvo, Eva; Watson, Andrew; Ríos, Aida F.; Pérez, Fiz F..
2015 Trends in anthropogenic CO2 in water masses of the Subtropical North Atlantic Ocean. *Progress in Oceanography*, 131. 21-32. 10.1016/j.pocean.2014.11.006

**Title page information**

**Title:**

# Trends in anthropogenic $CO_2$ in water masses of the Subtropical North Atlantic Ocean.

**Authors:**

Elisa F. Guallart[a,*], Ute Schuster[b], Noelia M. Fajar[c], Oliver Legge[d], Peter Brown[d,e], Carles Pelejero[a,f], Marie-Jose Messias[b], Eva Calvo[a], Andrew Watson[b], Aida F. Ríos[c] and Fiz F. Pérez[c].

**Address:**

[a]Institut de Ciències del Mar, CSIC, Pg. Marítim de la Barceloneta 37-49, E-08003, Barcelona, Spain.

[b]College of Life and Environmental Sciences, University of Exeter, Exeter, EX4 4PS, UK.

[c]Instituto de Investigacións Mariñas, CSIC, Eduardo Cabello 6, E-36208, Vigo, Spain.

[d]Centre for Ocean and Atmospheric Science, School of Environmental Sciences, University of East Anglia, Norwich, NR4 7TJ, UK.

[e]National Oceanography Centre, European Way, Southampton, SO14 3ZH, UK.

[f]Institució Catalana de Recerca i Estudis Avançats, Passeig Lluís Companys 23, E-08010, Barcelona, Spain.

[*]Corresponding author: Elisa F. Guallart

Tel: +34 93 230 9500; Fax: + 34 93 230 95 55

*E–mail addresses*: efernandez@icm.csic.es (E.F. Guallart), u.schuster@exeter.ac.uk (U. Shuster), nfajar@iim.csic.es (NM. Fajar), o.legge@uea.ac.uk (O. Legge), P.J.Brown@uea.ac.uk (P. Brown), carles.pelejero@icrea.cat (C. Pelejero), m.messias@exeter.ac.uk (MJ. Messias), , ecalvo@icm.csic.es (E. Calvo), andrew.watson@exeter.ac.uk (A. Watson), aida@iim.csic.es (A.F. Ríos), fiz.perez@iim.csic.es (F.F. Pérez).

## Abstract

The variability in the storage of the oceanic anthropogenic $CO_2$ ($C_{ant}$) on decadal timescales is evaluated within the main water masses of the Subtropical North Atlantic along 24.5°N. Inorganic carbon measurements on five cruises of the A05 section are used to assess the changes in $C_{ant}$ between 1992 and 2011, using four methods (ΔC*, TrOCA, $\varphi C_T^0$, TTD). We find good agreement between the $C_{ant}$ distribution and storage obtained using chlorofluorocarbons and $CO_2$ measurements in both the vertical and horizontal scales. $C_{ant}$ distribution shows higher concentrations and greater decadal storage rates in the upper layers with both values decreasing with depth. The greatest enrichment is obserbed in the central water masses, with their upper limb showing a mean annual accumulation of about 1 $\mu mol \cdot kg^{-1} \cdot yr^{-1}$ and the lower limb showing, on average, half that value. We detect zonal gradients in the accumulation of $C_{ant}$. This finding is less clear in the upper waters, where greater variability exists between methods. In accordance with data from time series stations, greater accumulation of $C_{ant}$ is observed in the upper waters of the western basin of the North Atlantic Subtropical Gyre. In intermediate and deep layers, the zonal gradient in the storage of $C_{ant}$ is more robust between methods. The much lower mean storage rates found along the section (< 0.25 $\mu mol \cdot kg^{-1} \cdot yr^{-1}$) become more obvious when longitudinal differences in the $C_{ant}$ accumulation are considered. In particular, west of 70°W the ventilation by the Labrador Sea Water creates a noticeable accumulation rate up to ~0.5 $\mu mol \cdot kg^{-1} \cdot yr^{-1}$ between 1000 and 2500 dbar. If a transient stationary state of the $C_{ant}$ distributions is considered, significant bi-decadal trends in the $C_{ant}$ storage rates in the deepest North Atlantic waters are detected, in agreement with recent estimations.



**Keywords:**

Anthropogenic $CO_2$; $C_{ant}$ storage rates; Decadal variability; $C_{ant}$ estimation; Steady State; Water masses.

Atlantic Ocean; Subtropical North Atlantic Gyre; DeepWestern Boundary Current.

**Abbreviations:**

| | |
|---|---|
| $C_{ant}$ | anthropogenic $CO_2$. |
| $[C_{ant}]$ | mean $C_{ant}$ concentrations, in µmol·kg$^{-1}$. |
| $[C_{ant}^{X}]$ | mean $C_{ant}$ values for method *X*, where *X* = $\varphi C_T^0$, TrOCA, ΔC* or TTD, in µmol·kg$^{-1}$. |
| DT(*X*) | Decadal Trend ± uncertainty in $C_{ant}$ accumulation for method *X*, where *X* = $\varphi C_T^0$, TrOCA, ΔC* or TTD, in µmol·kg$^{-1}$ yr$^{-1}$. |
| TSSR(*X*) | Transient Stationary State rate ± uncertainty in $C_{ant}$ accumulation for method *X*, where *X* = $\varphi C_T^0$, TrOCA, ΔC* or TTD, in µmol·kg$^{-1}$ yr$^{-1}$. |

# 1. Introduction

The ocean plays a major role as a sink for carbon dioxide ($CO_2$) released by humankind to the atmosphere, annually removing about a quarter of the total anthropogenic $CO_2$ ($C_{ant}$) emissions (Khatiwala et al., 2013). The North Atlantic Ocean plays an important part in absorbing and, especially, storing $C_{ant}$ (Watson et al., 1995; Vázquez-Rodríguez et al., 2009a; Pérez et al., 2010a). It contains up to 25% of the oceanic $C_{ant}$, although its surface represents only 13% of the global ocean (Sabine et al., 2004). Despite its large $C_{ant}$ storage rate, air-sea uptake in the North Atlantic is not predominantly anthropogenic, since natural $CO_2$ uptake largely prevails over the anthropogenic perturbation in the North Atlantic Subpolar Gyre (NASPG) (Pérez et al., 2013). The entrance of $C_{ant}$ into the ocean interior takes place in the NASPG through deep convection, significantly contributing to the efficiency of the North Atlantic sink. This $C_{ant}$ entrance is sustained up to 65±13% due to lateral transports that carry $C_{ant}$-loaded subtropical waters to these northern latitudes through the upper limb of the Meridional Overturning Circulation (MOC) (Álvarez et al., 2003; Macdonald et al., 2003; Rosón et al., 2003; Pérez et al., 2013). At 24.5ºN, the MOC is responsible for almost 90% of the meridional heat flux (Johns et al., 2011) and it also transports up to 0.17-0.20 $PgC \cdot y^{-1}$ of $C_{ant}$ (Macdonald et al., 2003; Rosón et al., 2003). Due to the importance of the North Atlantic Subtropical Gyre (NASTG) in the uptake of $C_{ant}$ from the atmosphere, the WOCE A05 hydrographic line, situated at 24.5°N, is suitable for the evaluation and quantification of the North Atlantic $C_{ant}$ sink. The A05 line has been studied several times using high spatial resolution *in situ* $CO_2$ system measurements performed in 1992 (Rosón *et al.*, 2003), 1998 (Macdonald *et al.*, 2003) and 2004 (Brown et al., 2010). Two recent occupations, in 2010 and 2011, add to this historical record.

Estimating $C_{ant}$ storage in the ocean is not simple because $C_{ant}$ is a small perturbation (3% at most) on top of natural, oceanic inorganic carbon ($C_T$). As $C_{ant}$ is not directly measurable it has to be estimated from indirect techniques using in-situ observations. Brewer (1978) and Chen and Millero (1979) presented the first $C_{ant}$ calculations in the late 1970s, which attempted to separate the $C_{ant}$ signal from the background $CO_2$ distribution by correcting the measured $C_T$ for changes due to biological activity and by removing an estimate of the preindustrial preformed $C_T$. Several authors have tried to improve those first back-calculation (also called carbon-based) methods, leading to a number of methodologies: ΔC*(Gruber et al.,

1996), $\Delta C_T^0$ (Kortzinger et al., 1998), TrOCA (Touratier and Goyet, 2004; Touratier et al., 2007) and $\varphi C_T^0$ (Vázquez-Rodríguez et al., 2009b). Overall, they rely on the assumption that ocean circulation and the biological pump have operated in steady state since the preindustrial era. In addition, other conceptual approaches (Broecker and Peng, 1974; Thomas and Ittekkot, 2001; Haine and Hall, 2002) do not use $C_T$ measurements and treat $C_{ant}$ as a conservative tracer (i.e. a tracer that is not influenced by biological processes in the ocean), avoiding the uncertainties related to the biological correction of the back-calculation methodologies. Tracer distributions can be established by using the so-called TTD functions (Transit Time Distributions). TTDs are mathematical expressions which serve to constrain the time elapsed since a water parcel was last in contact with the surface (Waugh et al., 2004; Waugh et al., 2006; Steinfeldt et al., 2009), to describe how the ocean's circulation connects and transports $C_{ant}$ from the surface to the ocean interior. Nevertheless, there is no clear consensus about the most appropriate method to estimate $C_{ant}$ (Sabine and Tanhua, 2010). While some authors have reported $C_{ant}$ estimates using only one method, $\Delta C^*$ (Macdonald et al., 2003; Rosón et al., 2003), TTD (Tanhua et al., 2008) or $\varphi C_T^0$ (Pérez et al., 2010a; Ríos et al., 2012), other authors have used two or more methods for comparative purposes: TrOCA and $\varphi C_T^0$ (Pérez et al., 2010b; Castaño-Carrera et al., 2012; Fajar et al., 2012), TrOCA, $\varphi C_T^0$ and $\Delta C^*$, (Flecha et al., 2012), $\Delta C^*$, $\Delta C_T^0$ and TrOCA (Lo Monaco et al., 2005) or $\Delta C^*$, TrOCA, $\Delta C_T^0$, TTD and $\varphi C_T^0$ (Vázquez-Rodríguez et al., 2009b). Moreover, some authors suggest that a combination of approaches is necessary to achieve a robust quantification of the ocean sink of $C_{ant}$ (Khatiwala *et al.*, 2013).

The A05 repeat section cruises provide a valuable time series to better constrain the decadal variability of the North Atlantic $C_{ant}$ storage from observational data. To this end, the present work studies the $C_{ant}$ changes between 1992 and 2011 along 24.5°N using four methods. Three back calculation methods ($\Delta C^*$ (Gruber et al., 1996), TrOCA (Touratier *et al.*, 2007) and $\varphi C_T^0$ (Vázquez-Rodríguez et al., 2009b)) and a tracer based technique (TTD (Waugh *et al.*, 2006)) are used to quantify the temporal changes in $C_{ant}$ concentrations within six different water masses of the Subtropical North Atlantic. This study also addresses possible longitudinal differences in the decadal $C_{ant}$ storage rates and provides a comparison of the results to a transient stationary state of oceanic $C_{ant}$ accumulation.

## 2. Data

Five repeats of the A05 hydrographic section are used to study the temporal evolution of $C_{ant}$ storage in the Subtropical North Atlantic Ocean (Table 1). The cruises in 1992, 1998 and 2004 are referred to as earlier cruises, compared to the two more recent occupations in 2010 and 2011. All the cruise tracks are shown in figure 1a: the 1992 occupation was carried out along 24.5°N, lying south of the later cruises at either end of the section and sampling the Florida Strait at 26°N. Subsequent occupations crossed the African shelf at approximately 28°N and the continental shelf off the Bahamas at 26.5°N, sampling the Florida Strait at 27°N. The 2010 cruise followed the Kane Fracture Zone, thus slightly deviating from the other cruise tracks across the Mid Atlantic Ridge (MAR).

### 2.1. Earlier cruises

Datasets from the earlier cruises are available on the CDIAC website (http://cdiac.ornl.gov/). The 1992 cruise was conducted under the framework of the WOCE Project. Procedures for $CO_2$ system parameters analyses and their adjustments are described in Rosón *et al.* (2003) and Guallart et al. (2013). The 1998 measurements are reported in Peltola et al. (2001) and Macdonald *et al.* (2003). Gaps in nutrient data in positions where $C_T$ and $A_T$ were available were filled using a multiparameter linear regression (MLR) technique (Velo et al., 2010).

In 2004, the section was reoccupied within the framework of the CLIVAR Program. The analysis methodologies are described in Cunningham (2005) and Brown *et al.* (2010). The 2004 dataset used in this work is a combination between the data available at CDIAC and the Florida Strait measurements available at the British Oceanographic Data Center (http://www.bodc.ac.uk/). Where $C_T$ was available and $A_T$ was not, interpolated normalized $A_T$ ($NA_T = A_T \cdot 35$ / salinity) was used in order to fill the gaps. The interpolation was performed on $NA_T$ data because they are less variable than $A_T$ (Millero et al., 1998).

### 2.2. Recent cruises

In 2010, the $C_T$ was measured by coulometry (Dickson et al., 2007) and $A_T$ was determined by potentiometric titration (Dickson *et al.*, 2007) using a VINDTA system (Marianda, Kiel, Germany). Certified reference material (CRM, batch 97) supplied by the Scripps Institution of

Oceanography was analysed twice every day. Accuracy was calculated as ±2.9 µmol·kg$^{-1}$ (n = 399) for $C_T$ and ±1.9 µmol·kg$^{-1}$ (n = 397) for $A_T$. After Secondary Quality Control (2ndQC) (Tanhua et al., 2010b) on $C_T$, $A_T$, nutrients and oxygen ($O_2$) data, $O_2$ and silicate were bias-adjusted (Table 1). The $C_T$ and $A_T$ data are further described in Schuster et al. (2013). The CFCs were measured at the LGMAC lab following Smethie *et al.* (2000) and Law *et al.* (1994). Nutrient gaps were filled as described above.

In 2011, the most recent occupation of the A05 section was carried out as part of the Circumnavigation Expedition MALASPINA 2010 (http://www.expedicionmalaspina.es/). The pH was measured spectrophotometrically (Clayton and Byrne, 1993) and $A_T$ was determined potentiometrically by titration at endpoint detection (Mintrop et al., 2000). $A_T$ gaps were filled as reported above. The $C_T$ was calculated from $A_T$ and pH using the dissociation constants of Mehrbach et al. (1973) refitted by Dickson and Millero (1987) using the CO2SYS program (Pierrot et al., 2006). Discrete $C_T$ samples were taken at 11 stations and analysed for quality control at the IIM-CSIC laboratory by coulometric determination using a SOMMA system (Johnson et al., 1998). The internal consistency between calculated and measured $C_T$ was estimated to be of 0.9 ± 3.5 µmol·kg$^{-1}$ (n=22). No adjustments were necessary after 2ndQC.

## 3. Methods

### 3.1. $C_{ant}$ determinations

Three back-calculation methods (ΔC*(Gruber et al., 1996), $\varphi C_T^0$ (Vázquez-Rodríguez et al., 2009b) and TrOCA (Touratier and Goyet, 2004; Touratier et al., 2007)) and one tracer-based method (TTD (Waugh et al., 2006)) were used to determine the $C_{ant}$ distributions. The overall uncertainties in $C_{ant}$ are ±9 µmol·kg$^{-1}$, ±5.2 µmol·kg$^{-1}$, ±6.25 µmol·kg$^{-1}$ and ±6 µmol·kg$^{-1}$ for ΔC*, $\varphi C_T^0$, TrOCA and TTD estimates, respectively. Further details on the specific assumptions of each of the four methodologies are provided in Appendix A, in the Supplementary Information.

### 3.2. Averaging by regions and layers

The five A05 datasets were divided vertically into six density layers and longitudinally into five regions (figure 1b). The water column was divided by identifying the main water masses representative of the Subtropical North Atlantic Ocean following Talley et al. (2011): North Atlantic Central Waters (NACW), Antarctic Intermediate Water (AAIW), North Atlantic Deep Waters (NADW) and Antarctic Bottom Water (AABW). The subducted thermocline (NACW) was further split into two main cores: the upper (uNACW), including a warm and saline component related to SubTropical Mode Water and the lower (lNACW), which is denser and fresher and related to SubPolar Mode Waters (McCartney and Talley, 1982). The boundary between AAIW and uNADW was also constrained according to the TS properties. Thus, the three uppermost layers were delimited using $\sigma_0$ along the isopycnals $\sigma_0$ = 26.7 kg·m$^{-3}$, $\sigma_0$ = 27.2 and $\sigma_0$ = 27.6 kg·m$^{-3}$, respectively (Fig.1b). The uNACW layer includes depths between ~150 - 450 dbar. Since the delimiting isopycnal is tilted up towards the east, this layer is far shallower on the eastern side of the section, where it reaches ~250 dbar. This layer shows the highest salinity in the water column, with an average of 36.6. The lNACW layer is located between ~250 and ~850 dbar. The top of the AAIW layer (from ~600 to ~1100 dbar) encompasses the oxygen minimum zone. The slight eastward salinization at these depths results from the influence of Mediterranean Water (MW), as it spreads through the layer below. The two NADW components were delimited according to a reference level of 2000 dbar ($\sigma_2$), along $\sigma_2$ = 37 kg·m$^{-3}$ (Fig.1b). The uNADW layer extends from ~1100 to ~2500 dbar. Its freshening close to the western margin is related to Labrador Sea Water (LSW) spreading. lNADW layer fills the eastern basin from ~2100 dbar to the ocean floor but extends to ~4500 dbar in the western basin. AABW was delimited in the western basin along the isopycnal $\sigma_4$ = 45.9 kg·m$^{-3}$. In addition to this classification of water masses, the section was zonally divided, separating the eastern and western basins at the Mid-Atlantic Ridge, at 45°W. The division of the western basin was refined in order to better constrain, in terms of its circulation features, the temporal variability of $C_{ant}$ distributions. The Florida Strait was identified as an independent region ranging from 80°W to 78°W. It was isolated from the main section due to its independent behaviour in terms of transports (Schmitz and Richardson, 1991; Macdonald et al., 2003; Rosón et al., 2003). The zone of deep ventilation by the Deep Western Boundary Current (DWBC), Region 1 (R1), was separated from the ocean interior at 70°W, isolating it from Region 2 (R2), where AABW fills a considerable volume of the deep

ocean. Despite not showing, *a priori*, distinct oceanographic features, the eastern basin was also halved at 30°W, separating Region 3 (R3) from Region 4 (R4) to isolate the relative salinity maximum of MW that enters the section from the African Coast.

These divisions result in a total of 25 boxes (Fig. 1b), within which the temporal variability of the mean $C_{ant}$ estimates was studied. Data above 150 dbar were removed to avoid seasonal biological effects, since conservative tracers do not vary seasonally in the subsurface (100-200m) (Vázquez-Rodríguez et al., 2012). Mean $C_{ant}$ values ($[C_{ant}^{X}]$, where $X$ = $\varphi C_T^0$, TrOCA, $\Delta C^*$ or TTD, in $\mu mol \cdot kg^{-1}$) within each box were computed as the mean and standard deviation of ensembles of 100 averages obtained through random perturbations of the $\varphi C_T^0$, TrOCA, $\Delta C^*$ and TTD estimates. Random perturbation of the data was performed using each method's uncertainty in order to propagate the uncertainty of the $C_{ant}$ estimates into the uncertainty of the box averages and the trends, independently of the number of data within each box. This led us to obtain means that were more robust but that did not change from the means obtained without perturbation calculations. This also permitted not using the error of the mean (of the raw data) as the uncertainty, which would have been lower in boxes with a large number of data. The values obtained are shown, for each cruise, in Appendix B of the Supplementary Information. Mean values ± standard error of the mean ($x \pm \sigma/\sqrt{N}$) of pressure (dbar), salinity, $O_2$ ($\mu mol \cdot kg^{-1}$), potential temperature ($\Theta$, ºC) and Apparent Oxygen Utilization (AOU, $\mu mol \cdot kg^{-1}$) within each box are also shown as Supporting Information of the $C_{ant}$ data.

### 3.3. Decadal trend and rate of change in $C_{ant}$ storage

#### 3.3.1. Decadal trend in $C_{ant}$ storage

In order to study the temporal changes in the mean $C_{ant}$ concentrations ($[C_{ant}]$) of $\varphi C_T^0$, TrOCA and $\Delta C^*$ within each box for the period 1992-2011, an ensemble of 100 linear regressions between the five years and the 100 random-perturbed averages was obtained. Linear regressions for TTD were performed from 1992 to 2010. The mean and the standard deviation of the 100 linear regressions were considered as the Decadal Trend (DT) and the uncertainty (in $\mu mol \cdot kg^{-1}\ yr^{-1}$) for $[C_{ant}]$ inside each box. As each $C_{ant}$ method yields a specific DT, hereafter they will be denoted as DT (method), e.g. DT($\varphi C_T^0$), DT(TrOCA), DT($\Delta C^*$)

and DT(TTD). Table C1 in the Supplementary Information shows the DT values in each box for each method.

### 3.3.2. Transient Steady State rate in $C_{ant}$ storage

Tanhua et al. (2006) found that $C_{ant}$ is in transient steady state (TSS) in the North Atlantic, from comparison of the observed changes in $C_T$ and CFC fields with those predicted from an eddy-permitting ocean circulation model. This means that $C_{ant}$ increases over time through the whole water column in a manner that is proportional to the time-dependent surface concentration. Hence, $C_{ant}$ changes for a given time period can be determined from [$C_{ant}$] (Tanhua et al., 2007; Steinfeldt et al., 2009; Khatiwala et al., 2013; Pérez et al., 2013) considering the exponential fit $C^0_{(t)} = Ae^{\lambda t}$ , that describes the history of atmospheric $CO_2$ and $C^0_{ant}$ in the ocean surface mixed layer since the Industrial Revolution. Steinfeldt et al. (2009) reported an annual rate increase of 1.69% for the factor $\lambda(yr^{-1})$, for characteristic NADW properties. The uncertainty associated to $\lambda$ was found to be 0.10%, based on the variability between 1992 and 2012 in the estimated rates of $C^0_{ant}$ increase in the surface mixed layer. The $C_{ant}$ storage rate ($\mu mol \cdot kg^{-1} \cdot yr^{-1}$) under a transient steady state can be calculated within each box as the product of $\lambda$ ($yr^{-1}$) and [$C_{ant}$] ($\mu mol \cdot kg^{-1}$), the [$C_{ant}$] term varying depending on the method used to estimate it:

$$\frac{dC_{ant}}{dt} = \lambda \cdot [C_{ant}] \quad (1)$$

To obtain robust $\frac{dC_{ant}}{dt}$ within each box, an ensemble of 100 $\frac{dC_{ant}}{dt}$ were obtained for each cruise using equation (1), from the 100 random-perturbed averages ([$C^{\varphi C^0_T}_{ant}$], [$C^{TrOCA}_{ant}$], [$C^{\Delta C^*}_{ant}$], [$C^{TTD}_{ant}$]) obtained as reported above and also considering the random perturbation of $\lambda$. Since all of the cruises were grouped to increase the amount of $\frac{dC_{ant}}{dt}$ estimations, the 100 random-perturbed averages relative to each cruise were time-normalized (Khatiwala et al., 2013) to the year 2000, using equation 2:

$$C_{(t2)} = C_{(t1)} e^{\lambda(t2-t1)} \quad (2)$$

where t1 corresponds to each A05 cruise occupation year and t2 is the reference year 2000. $C_{(t1)}$ corresponds to [$C_{ant}$] for each cruise, and $C_{(t2)}$ to the one normalized to year 2000. The temporal rescaling was performed to reduce the variability in the obtained storages due to the difference in [$C_{ant}$] between years, obtaining Transient steady state rates (TSSR) storages that were set in the middle of the studied period. The TSSR and its uncertainty were considered as the mean and standard deviation of the 500 $\frac{dC_{\mathrm{ant}}}{dt}$ (100 per cruise). Hereafter, the $C_{ant}$ storage rates (μmol·kg$^{-1}$ yr$^{-1}$) computed following the Transient Stationary State approximation will be denoted as TSSR (method), e.g. TSSR($\varphi C_T^0$), TSSR(TrOCA), TSSR(ΔC*) and TSSR(TTD). Table C1, in the Supplementary Information, shows the TSSR values in each box, for each method.

Taking into account that sometimes the $C_{ant}$ estimates from different methods extend over a broad range of values, Khatiwala et al., (2013) suggesed that a combination of $C_{ant}$ estimation methods, each with its own strengths and weaknesses, should be necessary to achieve a robust quantification of the ocean sink of $C_{ant}$. By applying their consideration to the $C_{ant}$ storage, table C1 shows the mean DT and TSSR within each box, where the four methods used to compute $C_{ant}$ are combined. Since DT uncertainties show a large variability between them, averaging was performed by weighting the mean from the three back-calculations, and then averaging this with the tracer method. The mean of the TSSR results was obtained by averaging the four methods without weighting them, because all of them showed much closer uncertainties. The time-normalized [$C_{ant}$] (to year 2000) obtained by averaging the four methods' estimates is also shown in table C1. The main objective of calculating the accumulation of $C_{ant}$ by these two different approaches was to compare the consistency between their results.

# 4. Results

## 4.1. Modern $C_{ant}$ distribution

Figure 2 shows the average vertical distributions of $C_{ant}^{\varphi C_T^0}$ in 1992 and 2011, for the eastern and western basins separately. All profiles show higher $C_{ant}^{\varphi C_T^0}$ values near the surface that decrease with depth. The vertical gradient is particularly strong in the upper ocean, from 150 to 1000 dbar, whilst concentrations remain low and almost constant below this. Below 1000 dbar, only the DWBC contributes to the deep ocean ventilation, mostly through the LSW spreading pathway. Its role can be identified as the relative maximum in $C_{ant}^{\varphi C_T^0}$ between 1100 and 1800 dbar, in the western basin. Temporal differences in the profiles reveal a substantial enrichment in $C_{ant}^{\varphi C_T^0}$ in both basins in the first 1000 dbar. This pressure range encompass the three uppermost density layers. Two of these water masses, uNACW and lNACW, show the largest accumulation detected in the water column and this accumulation is of a similar magnitude in each basin. In the deep ocean, $C_{ant}^{\varphi C_T^0}$ penetration occurs faster in the western basin than the eastern basin due to the DWBC spreading. It is difficult to discern changes in $C_{ant}^{\varphi C_T^0}$ below 2000 dbar as the uncertainty estimates overlap (Fig.2).

## 4.2. Decadal Trends in $C_{ant}$ storage by layer

### 4.2.1. uNACW ($\sigma_0$ < 26.5 kg m$^{-3}$)

All four $C_{ant}$ methods show the highest [$C_{ant}$] in uNACW, as it is the most ventilated layer (Fig.3). The range in [$C_{ant}$] between 1992 and 2011 is wide and depends on the method used, suggesting a rise of about ~ 10 - 22 µmol·kg$^{-1}$. The four methods show similar DT values in the eastern basin (R3 and R4, Fig. 4) but different DT in the $C_{ant}$ accumulation of the western basin (R1 and R2). There, DT (TTD) indicates much lower decadal increases in [$C_{ant}^{TTD}$] than the DT obtained using back-calculation methods. Thus, while [$C_{ant}^{\varphi C_T^0}$], [$C_{ant}^{TrOCA}$] and [$C_{ant}^{\Delta C^*}$] are estimated to have been increasing up to ~ 1 µmol·kg$^{-1}$ yr$^{-1}$, [$C_{ant}^{TTD}$] shows a smaller decadal increase (DT and TSSR values are reported in table C1 of the Supplementary Information). The TTD method typically produces the highest estimates in the upper layers (Vázquez-

Rodríguez et al., 2009a; Khatiwala et al., 2013). However, $[C_{ant}^{TTD}]$ gives similar values to the other three estimates in 1992, and progressively lower values in later years. The difference between $[C_{ant}^{TTD}]$ and the back-calculation results remains approximately constant between cruises in the layers below (Fig. 3). This can presumably be attributed to the decline in the atmospheric CFC concentrations since their peak during the past decade (Tanhua et al., 2008), which would lead to increasing underestimation of $[C_{ant}^{TTD}]$ in this layer (the most recently ventilated) with time during the study period.

### 4.2.2. lNACW ($26.5 < \sigma_0 < 27.1$ kg m$^{-3}$)

In each year, $[C_{ant}^{\varphi C_T^0}]$, $[C_{ant}^{TrOCA}]$, $[C_{ant}^{\Delta C^*}]$ and $[C_{ant}^{TTD}]$ in lNACW generally increase eastwards, coinciding with a higher ventilation due to tilting isopycnals (Fig. 3). This layer shows an increase in $[C_{ant}]$, of about ~ 6 to 11 µmol·kg$^{-1}$ when considering the four methods. All methods agree that R4 has the highest storage at this depth range (Fig. 4). Close to the western margin (R1), DT(TTD) suggests lower storage than back-calculations estimates. This can be explained by the decline in the atmospheric CFC concentrations (as in uNACW) and intense mixing with the layer above due to the winter outcrop (Bates, 2012).

### 4.2.3. AAIW ($27.1 < \sigma_0 < 27.5$ kg m$^{-3}$)

The four methods agree on greater storage in R1 than in the other regions (Fig. 4). DT($\varphi C_T^0$), DT(TrOCA) and DT(TTD) results show a similar longitudinal pattern: their high DT in R1 is reduced in the ocean interior (R2-R4) with quite similar DT values in R2 and R4 and a near absence of significant accumulation in R3. The stabilization of $[C_{ant}^{\varphi C_T^0}]$ and $[C_{ant}^{TrOCA}]$ in R3 (Fig. 3), seems to be a real feature and not an artefact of the methodologies used, since $[C_{ant}^{TTD}]$ does not show changes over time either. However, the values of DT(TTD) are low in general compared to back-calculations (Fig. 4). DT(ΔC*) results mostly agree with this zonal pattern but suggest a larger increase in $[C_{ant}^{\Delta C^*}]$ in R3 and R4. It is important to note that determining $C_{ant}$ in this layer is particularly difficult for a number of reasons. The AAIW layer includes biogeochemical features such as the $O_2$ minimum layer and it is strongly influenced by the dynamic water mass front between AAIW and MW and the coastal upwelling (Brown *et al.*, 2010). The different behaviour in $[C_{ant}^{\Delta C^*}]$ could be related to the fact that this method appears to be more sensitive than the other methods to shifts in Θ and $O_2$ horizons that occur in R3

and R4, in AAIW and uNADW (tables B3 and B4 in the Supplementary Information), which could have an effect on the computation of the disequilibrium term in these regions. It is therefore difficult to correctly compute [$C_{ant}$] or interpret its decadal trend at these depth ranges. The fact that the temporal evolution of the $C_{ant}$ averages along the AAIW layer practically parallels that of uNADW (Fig. 3) suggests that it might also be somewhat influenced by LSW $C_{ant}$ ventilation. Steinfeldt et al., (2007) also found a noticeable increase in CFC-12 concentration with time close to the western boundary, at depth ranges directly above the layer where the LSW spreads.

#### 4.2.4. uNADW ( $\sigma_0$> 27.5 and $\sigma_2$<37 kg m$^{-3}$)

The DT results from the four methods show significantly higher accumulation in R1 (up to ~ 8 to 11 µmol·kg$^{-1}$) than in other regions (Fig. 4). The DT values in R1 are similar to, or greater than in the layer above, with an increase of ~ 0.5 µmol·kg$^{-1}$ yr$^{-1}$. This value, which is comparable to the yearly $C_{ant}$ accumulation in lNACW and half of that in uNACW, indicates significant $C_{ant}$ advection at depth due to the LSW spreading. As reported above, the DT(ΔC*) results are somewhat higher than the other three methods in the eastern basin (Fig. 4), doubling [$C_{ant}^{\varphi C_T^0}$], [$C_{ant}^{TrOCA}$] and [$C_{ant}^{TTD}$] in R4. These three methods suggest storage rates slighltly above zero in R3.

#### 4.2.5. lNADW ( $\sigma_2$> 37 and $\sigma_4$<45.9 kg m$^{-3}$)

The magnitude of [$C_{ant}^{\Delta C^*}$], [$C_{ant}^{\varphi C_T^0}$], [$C_{ant}^{TrOCA}$] and [$C_{ant}^{TTD}$] are different in some regions (Fig. 3) but, nonetheless, their temporal trends are relatively consistent (Fig. 4). DT values from the four methods agree on a significant, albeit low, decadal increase in [$C_{ant}$] in R1, that amounts to about half of the annual increase in the layer above. ΔC* and TTD methods agree on a significant $C_{ant}$ accumulation in the entire western basin, while $\varphi C_T^0$ and TrOCA do not indicate any increase in R2 (Fig. 4). In the eastern basin, the four methods indicate that mean concentrations are significant (Fig. 3), but only the ΔC* results reveal significant accumulation of $C_{ant}$ in the basin during the last two decades (the TTD method supports this only in R4) (Fig. 4).

#### 4.2.6. AABW ($\sigma_4$>45.9 kg m$^{-3}$)

In this layer, changes in [$C_{ant}$] over time are negligible (Fig. 3). Although all four methods identify significantly non-zero $C_{ant}$ concentrations (mostly from 2004 onwards), the error bars are too large to confirm a significant rise in their concentrations. In R1, of the back-calculation methods, DT($\varphi C_T^0$) and DT(TrOCA) results suggest a small accumulation (Fig. 4) while [$C_{ant}^{TTD}$] remains almost constant in time (Fig. 3). In R2, DT results show no change over the last two decades. This could be representative of insignificant loadings of $C_{ant}$ in AABW at these latitudes. Alternatively, it could be related to the quantification limits of the methods applied, whereby the 19 year period investigated is currently insufficient to identify the small increases of $C_{ant}$ in these waters.

#### 4.2.7. Florida Strait

As shown in Figure 3, [$C_{ant}$] increases are observed in all three layers that move through the FS. Although larger differences are found in the [$C_{ant}$] estimates within the FS, DT results for uNACW and lNACW in this region show higher accumulations than the same water masses in R1. However, for the AAIW layer a much lower accumulation is identified for FS than in R1, particularly when using the TTD method. This can be explained by the respective origins of the three layers entering the FS compared to the those on the main section, according to Schmitz and Richardson (1991). Both uNACW and lNACW originate from the recirculation of the North Equatorial Current. The AAIW layer in the FS however, originates directly from the South Eastern Atlantic. While the two uppermost layers show similar $\Theta/S$ and oxygen values within R1, AAIW shows lower $\Theta/S$ and higher AOU values than AAIW on the main section (tables in Appendix B of the Supplementary Information). Thus, DT(TTD) suggests lower decadal increases than back-calculation methods (Fig. 4), as there is no increase in [$C_{ant}^{TTD}$] during the last two decades. Back-calculation DT results show consistent values throughout the water column in the FS, with the exception of DT($\varphi C_T^0$) that exhibits slightly lower values in the upper layers.

### 4.3. Comparison between Decadal Trends and Transient Stationary State rates in $C_{ant}$ storage by layers

Purple dashed lines in Figure 3 correspond to the mean TSSR ± its confidence interval, as reported in Table C1 of Appendix C. TSSR results represent the expected storage of $C_{ant}$ in each box, assuming that concentrations increase in agreement with the exponential increase of $C_{ant}$ in the surface ocean (see subsection 3.3.2). TSSR values thus follow the [$C_{ant}$] distribution (i.e. boxes containing higher concentrations are expected to also exhibit the highest storages, and accumulation rates decrease with depth or according to the progressively lower concentrations found in different layers). TSSR results generally show greater consistency between methods than they do for the DT approach, indicating that $[C_{ant}^{\varphi C_T^0}]$, $[C_{ant}^{TrOCA}]$, $[C_{ant}^{\Delta C^*}]$ and $[C_{ant}^{TTD}]$ estimations are similar between them. Although TSSR results do not always correspond well with those obtained from the DT approach (Fig. 4), they show much lower uncertainties (particularly in the deep ocean), due to the time-normalization of the data. This is the main benefit of using the TSSR approach. By referencing the mean [$C_{ant}$] of the five cruises to the year 2000 (values in table C1 in the Supplementary Information), possible biases in any single dataset are smoothed by averaging with the other years. The uncertainties of the obtained storages are therefore reduced, making them more robust. Although the DT approach is much more sensitive to the data quality of individual cruises (exemplified by the low number of data inputs (n=5) used to perform the linear regressions) it does allow the detection of a more realistic $C_{ant}$ storage rate for the 19 year study period. This is since changes are only computed using data from this time frame. Conversely, TSSR results need to be interpreted in terms of the total previous accumulative history of [$C_{ant}$], as storage is computed based on the exponential fit of the $C_{ant}$ increase at the surface since the preindustrial era. Thus possible real variations in the storage of $C_{ant}$ which deviate from a steady-state accumulation could become masked in the TSSR results due to its integration into the past accumulative history of $C_{ant}$.

The main objective of including the TSSR approach is to check whether $C_{ant}$ has been increasing at all depths along the section in accordance with the accumulation expected assuming a steady-state ocean. It is hoped that the inclusion of four $C_{ant}$ estimation methods in this comparison should make any inferences more robust. As TSSR results are interpreted as the expected theoretical steady accumulation of $C_{ant}$, any observed deviation from this using DT could be evidence that the accumulation of $C_{ant}$ has been impacted by recent changes in circulation or ventilation. Alternatively, when DT and TSSR outputs coincide, it could be

taken as an indication that the short-term (here bi-decadal) $C_{ant}$ storage (DT) is following a steady-state $C_{ant}$ storage (TSSR).

### 4.3.1. The upper ocean: uNACW, lNACW and AAIW

Central Waters (uNACW and lNACW) show progressively higher TSSR values from R1 to R4 (Fig. 4), suggesting a higher expected storage in the eastern than in the western basin. This pattern is in accordance with the [$C_{ant}$] distributions observed along the layers. For uNACW, TSSR and DT results from all methods compare well in R4, but start to progressively differ on moving westwards: while back-calculation TSSR outputs decrease slightly on moving from R3 to R1 (similar to [$C_{ant}$]), the corresponding DT results remain more or less equal ($\varphi C_T^0$) or even increase (TrOCA or $\Delta C^*$) (Fig. 4). For TTD, observed DT values suggest a lower [$C_{ant}^{TTD}$] accumulation towards the west while TSSR results indicate that similar accumulation should be expected along the layer. A significant difference between the DT and TSSR approaches is apparent for the four methods in the western basin: TTD outputs suggest that [$C_{ant}^{TTD}$] has been accumulating slower than expected, at least during the last two decades, while DT($\varphi C_T^0$), DT(TrOCA) and DT($\Delta C^*$) results suggest $C_{ant}$ concentrations have exceeded the expected steady-state increase. In contrast to this, the eastern basin shows decadal trends closer to a more stationary build-up. The most noticeable feature in lNACW is the stronger longitudinal gradient in storage rates between the eastern (higher) and the western (lower) basins for TSSR results than for DT results. This is due to the strong gradient in [$C_{ant}$] associated with the shallowing of isopycnals towards the east. However, only DT(TTD) shows the same pattern, as DT from back-calculation methods generally show greater coherence along the layer. In AAIW, TSSR values from the four methods match closely and indicate similar storages throughout the section (Fig. 4). This is in contrast to the DT results, that suggest greater accumulation in region R1. The expected TSSR storages in the ocean interior (R2 to R4) are mostly similar between the TTD and the back-calculated results.However, DT(TTD) outputs are generally lower than back-calculated DT results. The TSSR storages found from R2 to R4 are consistent to the observed DT values for $\varphi C_T^0$ and TrOCA. The only mismatch occurs in R3, where a TSSR storage similar to the surrounding regions is expected, as the $C_{ant}$ concentrations are significant, but neither [$C_{ant}^{\phi C_T^0}$], [$C_{ant}^{TrOCA}$] nor [$C_{ant}^{TTD}$] actually appear to have increased over the 19 year time period.

### 4.3.2. The deep ocean: uNADW, lNADW and AABW

In the deep layers (uNADW and lNADW) both approaches show R1 to be the region with the greatest build-up in $C_{ant}$, with TSSR results then exhibiting a smoother zonal gradient along the section than their respective DT values (Fig. 4) (primarily in uNADW). This result highlights the significant role of the DWBC in carrying high levels of $C_{ant}$ in the deeper western basin, especially in LSW (see below). The boxes of the ocean interior where [$C_{ant}$] are close to the detection limits show low but significant TSSR storages (Fig. 4), whereas the DT values are not always significant. This might be due to the inherent difficulty in accurately estimating $C_{ant}$ levels in deep waters and also identifying its temporal increase. It is thus difficult to ascertain if the absence of rising [$C_{ant}$] observed in the deep interior ocean (mainly in lNADW*)* is a real signal or a consequence of the time series simply not being long enough in duration. This issue is also relevant for AABW, where TSSR results show consistent storage rates in R1. For DT outputs, although significant levels of $C_{ant}$ are idenitified for all methods (Fig. 3), only $\varphi C_T^0$ and TrOCA show significant, non-zero rates (Fig. 4). TSSR results also suggest that significant $C_{ant}$ build-up could additionally be considered to be occurring in R2.

## 5. Discussion

The mean TSSR storage rate for the whole uNACW layer using all four methods gives an expected accumulation of 0.84 ± 0.07 $\mu mol \cdot kg^{-1} \cdot yr^{-1}$. The equivalent mean DT suggests a slightly higher observed value of 0.93 ± 0.09 $\mu mol \cdot kg^{-1} \cdot yr^{-1}$ (Fig. 4) that is mostly influenced by the significant dissimilarity between the two approaches in the western basin compared to the eastern basin, where DT values are closer to a steady-state accumulation. DT results from the back-calculation methods stand out; if only $\varphi C_T^0$, TrOCA and $\Delta C^*$ DT values were considered, these would suggest an even higher storage in the uppermost layer (1.07±0.08 $\mu mol \cdot kg^{-1} \cdot yr^{-1}$ on average), mainly due to the higher storage found in FS, R1 and R2 compared to those in R3 and R4.

Our findings are in accordance with those reported at time series stations in the Subtropical North Atlantic. Observations at BATS (Bermuda Atlantic Time-series Study), situated in the

Western Subtropical North Atlantic, suggest a three-decade trend (1983-2011) of 1.08 ± 0.06 $\mu mol \cdot kg^{-1} \cdot yr^{-1}$ for surface salinity-normalized $C_T$ ($nC_T$) (Bates et al., 2012). Conversely, at ESTOC (European Times Series Canary Islands), situated in the Eastern basin, a surface $nC_T$ storage rate of 0.99 ± 0.20 $\mu mol \cdot kg^{-1} \cdot yr^{-1}$ was reported (1995-2004) (Santana-Casiano et al., 2007). Although both values indicate an equivalent $nC_T$ storage when taking into account error estimates, a slightly increased $nC_T$ accumulation could be suggested for the western basin. In addition, based on $C_T$ and $A_T$ observations for Subtropical Mode Water (STMW, the main component of the uNACW layer in the western basin), Bates (2012) estimated a $C_{ant}$ storage rate of 1.06 $\mu mol \cdot kg^{-1} \cdot yr^{-1}$ between 1988 and 2011 at BATS. At ESTOC, the observed increase in $nC_T$ for the seasonal thermocline (around 120 m) amounted to 0.85 ± 0.16 $\mu mol \cdot kg^{-1} \cdot yr^{-1}$. This value matched the estimated $C_{ant}$ storage rate for the first 200 m obtained using the TrOCA method (González-Dávila et al., 2010). Furthermore, net $CO_2$ air-sea fluxes of -0.81 ± 0.25 to -1.3 ± 0.3 $mol \cdot m^2 \cdot yr^{-1}$ (1983 – 2005) and -0.051 ± 0.036 to -0.054 ± 0.03 $mol \cdot m^2 \cdot yr^{-1}$ (1995 – 2004), reported respectively for BATS (Bates, 2007) and ESTOC (Santana-Casiano et al., 2007), indicate that the eastern side of the NASTG has been acting as a much weaker sink for atmospheric $CO_2$ than the western side. These findings are consistent with previous results, where BATS was found to be in a region of strong spatial gradients in air-sea $CO_2$ flux (Nelson et al., 2001). In this context, our data suggest that during these two decades $C_{ant}$ may have been absorbed more intensely in the western side of the NASTG.

Circulation patterns additionally support these findings; STMW that forms near the Sargasso Sea both recirculates near its formation site and travels to the eastern NASTG through the Azores Current (Schmitz and Richardson, 1991; Follows et al., 1996). The larger amounts of $CO_2$ entering into the ocean near Bermuda (Bates, 2007) would be thus advected to the eastern part of the section below the surface. The transport of $C_{ant}$ enriched waters towards the east could explain the existence of higher [$C_{ant}$] at this side of the section (tables in appendix A), despite the lower $CO_2$ uptake rates reported there (Santana-Casiano *et al.*, 2007). It is important to note that there is no complete consensus among the four different methods used to evaluate the storage in $C_{ant}$ for uNACW in the western basin (Fig. 4). The TrOCA and $\Delta C^*$ methods suggest a faster DT in $C_{ant}$ moving closer to the west, while the $\varphi C_T^0$ method shows the same storage values throughout the layer. As highlighted above, the TTD method (that tends towards lower values in recent years) likely underestimates concentrations in this basin. Future updated trends for the $CO_2$ system parameters at ESTOC will help confirm whether

different accumulation rates have been occurring at each side of the NASTG. The annual mixing of lNACW with uNACW due to the winter outcrop in the west (Bates, 2012) could also favour the observed opposite TSSR and DT zonal gradients. This outcrop might favour lower [$C_{ant}$] closer to R1 due to mixing with less saturated underlying waters, mantaining a higher $C_{ant}$ uptake by uNACW at the western side of the section.

In contrast to central waters that show a general sustained long-term increase in [$C_{ant}$] values over their whole extent throughout the 19 year time period, the layers below (AAIW, NADW, AABW) show a generally divergent behaviour between the DT results in R1 and those in the ocean interior (R2-R4). The influence of the DWBC extends to R2 in most layers, resulting in contrasting DT between the western and eastern basins as a whole. In the AAIW layer, the greater rise in concentrations appears to occur in the western basin. Brown *et al.* (2010) pointed out that the variability in [$C_{ant}$] at these intermediate depths most likely results from changing mixing characteristics of waters of southern and Mediterranean origin, mainly due to a lateral movement of the water mass front that occurs between the AAIW and the MW. Regardless of the modulation of the $C_{ant}$ budget from the spreading of MW (Álvarez et al., 2005), the eastern basin shows almost no (R3) or only slight (R4) [$C_{ant}$] changes in time, which indicates that the observed DT storage rate for the whole AAIW ($0.22 \pm 0.08$ $\mu mol \cdot kg^{-1} \cdot yr^{-1}$) might have been mainly driven by R1. Although the higher weighted DT in R1 represents a relative minimum compared to those in lNACW and uNADW in the same region, it might have been mainly influenced by the $C_{ant}$ signal of the LSW spreading underneath (Steinfeldt *et al.*, 2007).

The prevailing role of R1 in the full section storage variability on decadal timescales becomes much more evident in deep waters below 1000 dbar (Macdonald et al., 2003; Brown et al., 2010). In the uNADW and lNADW layers, DT and TSSR results show storage rates that are higher in R1 than those further east (Fig. 4), due to the influence of recently ventilated waters moving southwards as part of the DWBC. These waters are enriched in $C_{ant}$ with respect to the less-ventilated layers that recirculate in the ocean interior (Steinfeldt et al., 2009; Pérez et al., 2010a), which themselves show small (uNADW) or not significant (lNADW) DT values. As reported above, the zonal gradient in the storage rates along the section is stronger for DT outputs than the TSSR approach due to their differing responses for LSW. The significantly higher storages observed (DT) for the period of study (Fig. 4) with respect to the expected

steady-state increase are confirmed by all four methods and can be explained by changes (increase) in deep-water ventilation owing to the strong renewal of LSW during the mid-1990s (Pérez et al., 2008). It is likely that we are detecting the arrival, at 24.5°N, of the greater amounts of $C_{ant}$ that entered into the subpolar gyre more than a decade ago, and have been transported southward by the DWBC.

With regards to AABW, weighted DT results in R1 show a non significant trend of about 0.11 ± 0.14 $\mu mol \cdot kg^{-1} \cdot yr^{-1}$ (Fig. 4), while those in R2 suggest no increase in [$C_{ant}$]. However, the corresponding TSSR values (0.12 ± 0.05 $\mu mol \cdot kg^{-1} \cdot yr^{-1}$ in R1 and 0.11 ± 0.04 $\mu mol \cdot kg^{-1} \cdot yr^{-1}$ in R2) suggest similar storages for the whole layer that are, in turn, equivalent to the observed DT results in R1. Ríos et al. (2012) reported a significant $C_{ant}$ storage rate of 0.15 ± 0.04 $\mu mol \cdot kg^{-1} \cdot yr^{-1}$ (1971 - 2003) in AABW in the Western South Atlantic (55ºS-10N). For this same basin, Wanninkhof et al. (2013) were able to detect, from $pCO_2$ measurements, small $C_T$ changes in deep waters from 44°S to the Equator, obtaining a storage rate of 0.47 $mol \cdot m^2 \cdot yr^{-1}$ for depths under 2000 m. Considering an average thickness of the water column of about ~3000 m (from ~2000 m to the ocean bottom) it can be deduced that they found storage rates equivalent to ~0.15 $\mu mol \cdot kg^{-1} \cdot yr^{-1}$, that are applicable to deep and bottom water masses at these latitudes in the North Atlantic, in agreement with Ríos et al.(2012). Both results are consistent with the mean TSSR values obtained in the AABW (table C1 in Appendix C), which indicate the expected storage according to the estimated [$C_{ant}$] in this layer. Only the weighted DT in R1 appears to confirm this. In addition, a mean TSSR of 0.12 ± 0.05 $\mu mol \cdot kg^{-1} \cdot yr^{-1}$ is also obtained for the whole lNADW layer, which is also consistent with Ríos et al. (2012) and Wanninkhof et al. (2013). Only DT(TTD) and DT(ΔC*) suggest similar results for the lNADW layer in R2 (table C1 in Appendix C). Brown et al. (2010) described a significantly non-zero $C_{ant}$ signal at 24.5°N for depth ranges between 4000 - 6000 dbar in the deep eastern basin (Fig 7 in Brown et al.(2010)), that was confirmed from $CCl_4$ measurements. These authors suggested that these [$C_{ant}$] levels might be related to the arrival of ventilated waters from the North along the eastern flank of the Mid-Atlantic Ridge, which Paillet and Mercier (1997) described as Iceland-Scotland Overflow Water. Roughly, it would correspond to an approximate storage of about ~ 0.2 - 0.3 $\mu mol \cdot kg^{-1} \cdot yr^{-1}$, which is consistent with our results, given the fact that our storage is referred to a layer with almost double the thickness (between 2500- 5500 dbar).

Differences in the storage rates found between methods were more evident where the $C_{ant}$ detection limits became more important. In deep homogeneous waters with very low $C_{ant}$, absolute uncertainties were of the same order of magnitude as the $C_{ant}$ concentrations, making significant trends difficult to separate from the background noise on a timescale of two decades. This is the case for lNADW and AABW, where there was no obvious accumulation of $C_{ant}$ (considering the uncertainties) despite the fact that the estimated $C_{ant}$ content could be considered to be significant. Here, we found significant bi-decadal trends in the $C_{ant}$ storage rates of the deepest Subtropical North Atlantic waters by using all five A05 datasets and the assumption of a transient steady state of the $C_{ant}$ distributions, in order to reduce the uncertainties related to deep waters measurements. Our results are consistent with Ríos et al. (2012), who used the same methodology as in our study ($C_T$ and $A_T$ measurements), but a larger timescale (three decades), to compute the $C_{ant}$ storage in the Western South Atlantic basin. Our findings also match those obtained by Wanninkhof et al. (2013), who studied the $C_{ant}$ change along the entire Atlantic Ocean during a period of time similar to ours, almost two decades, but with more precise $pCO_2$ measurements.

## 6. Conclusions

The $CO_2$ system measurements from the most recent occupations of the A05 section across 24.5°N in the Subtropical North Atlantic in 2010 and 2011 were compared with data from the three previous cruises. These five sections permitted the estimation of the $C_{ant}$ storage on decadal timescales within the main water masses present at the section. To better constrain the accumulation of $C_{ant}$, this was estimated by using four different methods that include back-calculation ($\Delta C^*$, TrOCA and $\varphi C_T^0$) and tracer (TTD) principles. Regardless of the method used to estimate [$C_{ant}$], the overall distribution showed higher $C_{ant}$ concentrations near the surface that decreased towards the bottom. By investigating the accumulation of $C_{ant}$ in different water masses along the section, we found that the greatest decadal storage rates were observed in the central water masses. uNACW showed a mean storage rate close to ~1 $\mu mol \cdot kg^{-1} \cdot yr^{-1}$ and lNACW displayed ~0.5 $\mu mol \cdot kg^{-1} \cdot yr^{-1}$, on average. Our results for uNACW are in accordance with the reported storage rates of $C_{ant}$ and $nC_T$ at BATS (Bates, 2012) and ESTOC (González-Dávila *et al.*, 2010) time series stations. Below the central

layers, neither intermediate nor deep water masses showed average storage rates greater than ~0.25 μmol·kg$^{-1}$·yr$^{-1}$. Zonal gradients in the accumulation of $C_{ant}$ were detected throughout the water column, with robust results identified for intermediate and deep water masses. The four methods gave evidence of higher storages of $C_{ant}$ occurring close to the western continental slope due to the conveyer role of the DWBC, in comparison with the low storage rates of the ocean interior. In particular, the storage rate of the uNADW layer within the DWBC region amounted to ~0.5 μmol·kg$^{-1}$·yr$^{-1}$ due to the contribution of recently ventilated LSW. In the upper layers (mode waters), the zonal gradient was less clear due to the greater variability that existed between the different methods of $C_{ant}$ estimaton. Results suggest that, at least for the period of study, $C_{ant}$ might have been absorbed more intensely in the western side of the NASTG, although more evidence is needed to confirm this.

For the vast majority, the four methods gave consistent storage rates indicating a good agreement between tracer and $CO_2$-based results. However, some differences in the obtained storage rates were observed: the TTD method may have underestimated storages in the two uppermost layers (mode waters). The ΔC* method gave decadal storage values slightly higher than the other three methods in the eastern basin in intermediate and deep layers, which likely results from the estimation of its disequilibria. The $C_{ant}$ accumulation calculated by using TrOCA method usually lied between the ΔC* and $\varphi C_T^0$ results, with the latter method indicating storage rates closer to the TTD method. There was generally better agreement between the storage rates of the four methods in the layers where the estimation of $C_{ant}$ is more robust. Agreement between the four methods was found in regions where the recent evolution of $C_{ant}$ for the period 1992- 2011 (DT results) appeared similar to the expected steady behaviour of the $C_{ant}$ distributions (TSSR results), suggesting that the accumulation of $C_{ant}$ was not impacted by recent changes in circulation. However, the four methods exhibited greater variability in regions where DT results suggested a departure from a transient steady state behaviour of the ocean. Due to the steady-state assumption inherent in each different $C_{ant}$ estimation technique, this observed variability will make it more difficult in the coming years to consistently track and constrain the oceanic $C_{ant}$ increase.

The A05 repeat hydrography thus permits the robust estimation of the storage of $C_{ant}$ on decadal timescales and allows a better constraint of the interactions between the ocean

circulation and the carbon cycle, in particular regarding the mechanisms governing the accumulation of $C_{ant}$ in the Subtropical North Atlantic.

## Acknowledgements

We would like to thank captains, officers and crews of RRS Discovery and R/V Sarmiento de Gamboa and the scientific and technical teams for their support and indispensable help during the cruises in 2010 and 2011. We acknowledge funding from the Spanish Ministry of Economy and Competitiveness through grants CSD2008-00077 (Circumnavigation Expedition MALASPINA 2010 Project), CTM2009-08849 (ACDC Project) and CTM2012-32017 (MANIFEST Project). We also acknowledge funding from the EU FP7 project CARBOCHANGE under grant agreement no. 264879 and by the Marine Biogeochemistry and Global Change research group (Generalitat de Catalunya, 2014SGR1029). E.F. Guallart was funded through a JAE-Pre grant that was financed by the Spanish National Research Council Agency (Consejo Superior de Investigaciones Científicas, CSIC) and by the European Social Fund.

## References

Álvarez, M., Pérez, F.F., Shoosmith, D.R., Bryden, H.L., 2005. Unaccounted role of Mediterranean Water in the drawdown of anthropogenic carbon. Journal of Geophysical Research: Oceans (1978–2012), 110.

Álvarez, M., Ríos, A.F., Pérez, F.F., Bryden, H.L., Rosón, G., 2003. Transports and budgets of total inorganic carbon in the subpolar and temperate North Atlantic. Global Biogeochemical Cycles, 17, 1002.

Bates, N.R., 2007. Interannual variability of the oceanic CO2 sink in the subtropical gyre of the North Atlantic Ocean over the last 2 decades. Journal of Geophysical Research: Oceans, 112, C09013.

Bates, N.R., 2012. Multi-decadal uptake of carbon dioxide into subtropical mode water of the North Atlantic Ocean. Biogeosciences, 9, 2649-2659.

Bates, N.R., Best, M.H.P., Neely, K., Garley, R., Dickson, A.G., Johnson, R.J., 2012. Detecting anthropogenic carbon dioxide uptake and ocean acidification in the North Atlantic Ocean. Biogeosciences 9, 2509-2522.

Brewer, P.G., 1978. Direct observation of the oceanic CO2 increase. Geophysical Research Letters, 5, 997-1000.

Broecker, W.S., Peng, T.H., 1974. Gas exchange rates between air and sea. Tellus, 26, 21-35.

Brown, P.J., Bakker, D.C.E., Schuster, U., Watson, A.J., 2010. Anthropogenic carbon accumulation in the subtropical North Atlantic. Journal of Geophysical Research-Oceans, 115, 4016.

Castaño-Carrera, M., Pardo, P.C., Álvarez, M., Lavín, A., Rodríguez, C., Carballo, R., Ríos, A.F., Pérez, F.F., 2012. Anthropogenic carbon and water masses in the bay of Biscay. Scientia Marina, 38, 191-207.

Chen, G.T., Millero, F.J., 1979. Gradual increase of oceanic CO2. Nature, 277, 205-206.

Clayton, T.D., Byrne, R.H., 1993. Spectrophotometric seawater pH measurements: total hydrogen ion concentration scale calibration of m-cresol purple and at-sea results. Deep Sea Research Part I: Oceanographic Research Papers, 40, 2115-2129.

Cunningham, S.A., 2005. Cruise Report No. 54. RRS Discovery Cruise D279, 04 Apr - 10 May 2004. A Transatlantic hydrographic section at 24.5ºN. . Southampton Oceanography Centre.

Dickson, A.G., Millero, F.J., 1987. A comparison of the equilibrium constants for the dissociation of carbonic acid in seawater media. Deep Sea Research Part A. Oceanographic Research Papers 34, 1733-1743.

Dickson, A.G., Sabine, C.L., Christian, J.R., 2007. Guide to best practices for ocean $CO_2$ measurements.

Fajar, N.M., Pardo, P.C., Carracedo, L., Vázquez-Rodríguez, M., Ríos, A.F., Pérez, F.F., 2012. Trends of anthropogenic CO2 along 20°W in the Iberian Basin. Scientia Marina, 38, 287-306.

Flecha, S., Pérez, F.F., Navarro, G., Ruiz, J., Olivé, I., Rodríguez-Gálvez, S., Costas, E., Huertas, I.E., 2012. Anthropogenic carbon inventory in the Gulf of Cádiz. Journal of Marine Systems, 92, 67-75.

Follows, M.J., Williams, R.G., Marshall, J.C., 1996. The solubility pump of carbon in the subtropical gyre of the North Atlantic. Journal of Marine Research, 54, 605-630.

González-Dávila, M., Santana-Casiano, J.M., Rueda, M.J., Llinás, O., 2010. The water column distribution of carbonate system variables at the ESTOC site from 1995 to 2004. Biogeosciences 7, 3067-3081.

Gruber, N., Sarmiento, J.L., Stocker, T.F., 1996. An improved method for detecting anthropogenic CO2 in the oceans. Global Biogeochemical Cycles, 10, 809-837.

Guallart, E.F., Pérez, F.F., Rosón, G., Ríos, A.F., 2013. High spatial resolution alkalinity and pH measurements by IIM-CSIC group along 24.5°N during the R/V Hespérides WOCE Section A05 cruise. (July 14 - August 15, 1992). Oak Ridge, Tennessee: Carbon Dioxide Information Analysis Center, Oak Ridge National Laboratory, US Department of Energy.

Haine, T.W.N., Hall, T.M., 2002. A Generalized Transport Theory: Water-Mass Composition and Age. Journal of Physical Oceanography, 32, 1932.

Johns, W.E., Baringer, M.O., Beal, L.M., Cunningham, S.A., Kanzow, T., Bryden, H.L., Hirschi, J.J.M., Marotzke, J., Meinen, C.S., Shaw, B., Curry, R., 2011. Continuous, Array-Based Estimates of Atlantic Ocean Heat Transport at 26.5°N. Journal of Climate, 24, 2429-2449.

Johnson, K.M., Dickson, A.G., Eischeid, G., Goyet, C., Guenther, P., Key, R.M., Millero, F.J., Purkerson, D., Sabine, C.L., Schottle, R.G., Wallace, D.W.R., Wilke, R.J., Winn, C.D., 1998. Coulometric total carbon dioxide analysis for marine studies: Assessment of the quality of total inorganic carbon measurements made during the US Indian Ocean CO2 survey 1994-1996. Marine Chemistry, 63, 21-37.

Khatiwala, S., Tanhua, T., Mikaloff Fletcher, S., Gerber, M., Doney, S.C., Graven, H.D., Gruber, N., McKinley, G.A., Murata, A., Ríos, A.F., Sabine, C.L., Sarmiento, J.L., 2013. Global ocean storage of anthropogenic carbon. Biogeosciences, 10, 2169-2191.

Körtzinger, A., Mintrop, L., Duinker, J.C., 1998. On the penetration of anthropogenic CO2 into the North Atlantic Ocean. Journal of Geophysical Research: Oceans, 103, 18681-18689.

Law, C.S., Watson, A.J., Liddicoat, M.I., 1994. Automated vacuum analysis of sulphur hexafluoride in seawater: derivation of the atmospheric trend (1970–1993) and potential as a transient tracer. Marine Chemistry, 48, 57-69.

Lo Monaco, C., Goyet, C., Metzl, N., Poisson, A., Touratier, F., 2005. Distribution and inventory of anthropogenic CO2 in the Southern Ocean: Comparison of three data-based methods. Journal of Geophysical Research C: Oceans, 110, 1-12.

Macdonald, A.M., Baringer, M.O., Wanninkhof, R., Lee, K., Wallace, D.W.R., 2003. A 1998–1992 comparison of inorganic carbon and its transport across 24.5°N in the Atlantic. Deep Sea Research Part II: Topical Studies in Oceanography, 50, 3041-3064.

McCartney, M.S., Talley, L.D., 1982. The Subpolar Mode Water of the North Atlantic Ocean. Journal of Physical Oceanography, 12, 1169-1188.

Mehrbach, C., Culberson, C.H., Hawley, J.E., Pytkowicz, R.M., 1973. Measurement of the Apparent Dissociation Constants of Carbonic Acid in Seawater at Atmospheric Pressure. Limnology and Oceanography, 18, 897-907.

Millero, F.J., Lee, K., Roche, M., 1998. Distribution of alkalinity in the surface waters of the major oceans. Marine Chemistry, 60, 111-130.

Mintrop, L., Pérez, F.F., Gonzalez-Dávila, M., Santana-Casiano, J.M., Körtzinger, A., 2000. Alkalinity determination by potentiometry: intercalibration using three different methods. Ciencias Marinas, 26(1), 23-27.

Nelson, N.B., Bates, N.R., Siegel, D.A., Michaels, A.F., 2001. Spatial variability of the CO2 sink in the Sargasso Sea. Deep Sea Research Part II: Topical Studies in Oceanography, 48, 1801-1821.

Paillet, J., Mercier, H., 1997. An inverse model of the eastern North Atlantic general circulation and thermocline ventilation. Deep Sea Research Part I: Oceanographic Research Papers, 44, 1293-1328.

Peltola, E., Lee, K., Wanninkhof, R., Feely, R., Roberts, M., Greeley, D., Baringer, M., Johnson, G., Bullister, J., Mordy, C., Zhang, J.-Z., P. Quay, F., Millero, F., Hansell, D., Minnett, P., 2001. Chemical and Hydrographic measurements on a climate and global change cruise along 24ºN in the Atlantic Ocean Woce Section A5R(repeat) during JAnuary-February 1998. Miami, Florida: Atlantic Oceanographic and Meteorological Laboratory. .

Pérez, F.F., Vázquez-Rodríguez, M., Mercier, H., Velo, A., Lherminier, P., Ríos, A.F., 2010a. Trends of anthropogenic CO2 storage in North Atlantic water masses. Biogeosciences, 7, 1789-1807.

Pérez, F.F., Aristegui, J., Vázquez-Rodríguez, M., Ríos, A.F., 2010b. Anthropogenic CO2 in the Azores region. Scientia Marina, 74, 11-19.

Pérez, F.F., Vázquez-Rodríguez, M., Louarn, E., Padín, X.A., Mercier, H., Ríos, A.F., 2008. Temporal variability of the anthropogenic CO2 storage in the Irminger Sea. Biogeosciences 5 (6), 1669-1679.

Pérez, F.F., Mercier, H., Vázquez-Rodríguez, M., Lherminier, P., Velo, A., Pardo, P.C., Rosón, G., Ríos, A.F., 2013. Atlantic Ocean CO2 uptake reduced by weakening of the meridional overturning circulation. Nature Geoscience, 6, 146-152.

Pierrot, D., Lewis, E., Wallace, D., 2006. MS Excel Program Developed for $CO_2$ System Calculations, ORNL/CDIAC-105a. Carbon Dioxide Information Analysis Center, Oak Ridge National Laboratory, US Department of Energy, Oak Ridge, Tennessee.

Ríos, A.F., Velo, A., Pardo, P.C., Hoppema, M., Pérez, F.F., 2012. An update of anthropogenic CO 2 storage rates in the western South Atlantic basin and the role of Antarctic Bottom Water. Journal of Marine Systems, 94, 197-203.

Rosón, G., Ríos, A.F., Pérez, F.F., Lavín, A., Bryden, H.L., 2003. Carbon distribution, fluxes, and budgets in the subtropical North Atlantic Ocean (24.5°N). Journal of Geophysical Research: Oceans, 108, n/a-n/a.

Sabine, C.L., Feely, R.A., Gruber, N., Key, R.M., Lee, K., Bullister, J.L., Wanninkhof, R., Wong, C.S., Wallace, D.W.R., Tilbrook, B., Millero, F.J., Peng, T.-H., Kozyr, A., Ono, T., Rios, A.F., 2004. The oceanic sink for anthropogenic $CO_2$. Science, 305, 367-371.

Sabine, C.L., Tanhua, T., 2010. Estimation of Anthropogenic CO2 Inventories in the Ocean. Annual Review of Marine Science, 2, 175-198.

Santana-Casiano, J.M., González-Dávila, M., Rueda, M.-J., Llinás, O., González-Dávila, E.-F., 2007. The interannual variability of oceanic CO2 parameters in the northeast Atlantic subtropical gyre at the ESTOC site. Global Biogeochemical Cycles, 21, GB1015.

Schmitz Jr.W.J., Richardson, P.L., 1991. On the sources of the Florida Current. Deep Sea Research Part A. Oceanographic Research Papers, 38, Supplement 1, S379-S409.

Schuster, U., Watson, A.J., Bakker, D.C.E., de Boer, A.M., Jones, E.M., Lee, G.A., Legge, O., Louwerse, A., Riley, J., Scally, S., 2013. Measurements of total alkalinity and inorganic dissolved carbon in the Atlantic Ocean and adjacent Southern Ocean between 2008 and 2010. Earth Syst. Sci. Data Discuss., 6, 621-639.

Smethie, W.M., Schlosser, P., Bönisch, G., Hopkins, T.S., 2000. Renewal and circulation of intermediate waters in the Canadian Basin observed on the SCICEX 96 cruise. Journal of Geophysical Research: Oceans, 105, 1105-1121.

Steinfeldt, R., Rhein, M., Bullister, J.L., Tanhua, T., 2009. Inventory changes in anthropogenic carbon from 1997–2003 in the Atlantic Ocean between 20°S and 65°N. Global Biogeochemical Cycles, 23, GB3010.

Steinfeldt, R., Rhein, M., Walter, M., 2007. NADW transformation at the western boundary between and. Deep Sea Research Part I: Oceanographic Research Papers, 54, 835-855.

Stendardo, I., Gruber, N., Körtzinger, A., 2009. CARINA oxygen data in the Atlantic Ocean. Earth system science data, 1, 87-100.

Talley, L.D., Pickard, G.L., Emery, W.J., Swift, J.H., 2011. Chapter 9 - Atlantic Ocean. *Descriptive Physical Oceanography (Sixth Edition)* (pp. 245-301). Boston: Academic Press.

Tanhua, T., Biastoch, A., Körtzinger, A., Lüger, H., Böning, C., Wallace, D.W.R., 2006. Changes of anthropogenic CO2 and CFCs in the North Atlantic between 1981 and 2004. Global Biogeochemical Cycles, 20, GB4017.

Tanhua, T., Körtzinger, A., Friis, K., Waugh, D.W., Wallace, D.W.R., 2007. An estimate of anthropogenic CO2 inventory from decadal changes in oceanic carbon content. Proceedings of the National Academy of Sciences, 104, 3037-3042.

Tanhua, T., Steinfeldt, R., Key, R.M., Brown, P., Gruber, N., Wanninkhof, R., Pérez, F., Körtzinger, A., Velo, A., Schuster, U., van Heuven, S., Bullister, J.L., Stendardo, I.,

Hoppema, M., Olsen, A., Kozyr, A., Pierrot, D., Schirnick, C., Wallace, D.W.R., 2010a. Atlantic Ocean CARINA data: overview and salinity adjustments. Earth system science data, 2, 17-34.

Tanhua, T., van Heuven, S., Key, R.M., Velo, A., Olsen, A., Schirnick, C., 2010b. Quality control procedures and methods of the CARINA database. Earth system science data, 2, 35-49.

Tanhua, T., Waugh, D.W., Wallace, D.W.R., 2008. Use of SF6 to estimate anthropogenic CO2 in the upper ocean. Journal of Geophysical Research C: Oceans, 113.

Thomas, H., Ittekkot, V., 2001. Determination of anthropogenic CO2 in the North Atlantic Ocean using water mass ages and CO2 equilibrium chemistry. Journal of Marine Systems, 27, 325-336.

Touratier, F., Azouzi, L., Goyet, C., 2007. CFC-11, Δ14C and 3H tracers as a means to assess anthropogenic CO2 concentrations in the ocean. Tellus, Series B: Chemical and Physical Meteorology, 59, 318-325.

Touratier, F., Goyet, C., 2004. Definition, properties, and Atlantic Ocean distribution of the new tracer TrOCA. Journal of Marine Systems, 46, 169-179.

Vázquez-Rodríguez, M., Padin, X.A., Pardo, P.C., Ríos, A.F., Pérez, F.F., 2012. The subsurface layer reference to calculate preformed alkalinity and air–sea CO2 disequilibrium in the Atlantic Ocean. Journal of Marine Systems, 94, 52-63.

Vázquez-Rodríguez, M., Touratier, F., Lo Monaco, C., Waugh, D.W., Padin, X.A., Bellerby, R.G.J., Goyet, C., Metzl, N., Ríos, A.F., Pérez, F.F., 2009a. Anthropogenic carbon distributions in the Atlantic Ocean: data-based estimates from the Arctic to the Antarctic. Biogeosciences, 6, 439-451.

Vázquez-Rodríguez, M., Padin, X.A., Ríos, A.F., Bellerby, R.G.J., Pérez, F.F., 2009b. An upgraded carbon-based method to estimate the anthropogenic fraction of dissolved CO2 in the Atlantic Ocean. Biogeosciences Discuss., 6, 4527.

Velo, A., Vázquez-Rodríguez, M., Padín, X.A., Gilcoto, M., Ríos, A.F., Pérez, F.F., 2010. A multiparametric method of interpolation using WOA05 applied to anthropogenic CO2 in the atlantic. Scientia Marina, 74, 21-32.

Wanninkhof, R., Park, G.-H., Takahashi, T., Feely, R.A., Bullister, J.L., Doney, S.C., 2013. Changes in deep-water CO2 concentrations over the last several decades determined from discrete pCO2measurements. Deep Sea Research Part I: Oceanographic Research Papers, 74, 48-63.

Watson, A.J., Nightingale, P.D., Cooper, D.J., 1995. Modelling atmosphere-ocean CO2 transfer. Philosophical Transactions - Royal Society of London, B, 348, 125-132.

Waugh, D.W., Haine, T.W.N., Hall, T.M., 2004. Transport times and anthropogenic carbon in the subpolar North Atlantic Ocean. Deep-Sea Research Part I: Oceanographic Research Papers, 51, 1475-1491.

Waugh, D.W., Hall, T.M., McNeil, B.I., Key, R., Matear, R.J., 2006. Anthropogenic CO2 in the oceans estimated using transit time distributions. Tellus, Series B: Chemical and Physical Meteorology, 58, 376-389.

Yool, A., Oschlies, A., Nurser, A.J.G., Gruber, N., 2010. A model-based assessment of the TrOCA approach for estimating anthropogenic carbon in the ocean. Biogeosciences, 7, 723-751.

**Table 1.** Cruises information on the repeat section A05.

| Cruise name (Expocode) | Dataset | Year | Period | Research Vessel | Sampled stations | $CO_2$ parameters[a] | Carbon related data PI(s) | Data adjustments in this study ($\mu mol \cdot kg^{-1}$) |
|---|---|---|---|---|---|---|---|---|
| 29HE06_1-3 | GLODAP | **1992** | 7/14 -8/15 | *R/V Bio Hespérides* | 112 | $A_T$(m), pH(m), $C_T$ (calc) | F. Millero /A. Ríos | $A_T$(+4)[b] pH(-0.009 units)[b] |
| 33RO19980123 | CARINA | **1998** | 1/23-2/24 | *R/V Ronald H. Brown* | 130 | $A_T$(m), pH(m), $C_T$(m) | R. Wanninkhof/ R.Feely | $O_2$(*0.99)[c] |
| 74DI20040404 | CARINA own data | **2004** | 4/4-5/10 | *R/V Discovery* | 125 | $A_T$(m), $C_T$(m) | U. Schuster | $SiO_4$ (*0.98)[d] $NO_3$ (*0.97)[d] |
| 74DI20100106 | New data[e] | **2010** | 1/6-2/18 | *R/V Discovery* | 135 | $A_T$(m), $C_T$(m) | U. Schuster | $O_2$(*1.03)[f] SiO4 (*0.94)[f] |
| -- | New data | **2011** | 1/28-3/14 | *R/V Sarmiento de Gamboa* | 167 | $A_T$(m), pH(m), $C_T$ (calc) | E F. Guallart/F.F. Pérez | -- |

[a] (m) = measured parameter, (calc) = calculated parameter.

[b](Guallart *et al.*, 2013)

[c](Stendardo *et al.*, 2009)

[d](Tanhua et al., 2010a)

[e](Schuster *et al.*, 2013)

[f] this study

Figure captions

**Figure 1. a)** A05 section tracks for the 1992 (green), 1998 (red), 2004 (dark blue), 2010 (light blue) and 2011 (yellow) cruises. **b)** Regions, layers and defined boxes over the salinity distribution of the 2011 cruise. The sections were zonally divided into five regions: Region 0 (Florida Strait, 80°W to 78°W), region 1 (78°W to 70°W), region 2 (70°W to 45°W), region 3 (45°W to 30°W) and region 4 (30°W to 10°W). Six density layers were defined identifying the main water masses of the Subtropical North Atlantic: uNACW ($\sigma_0$<26.7 kg·m$^{-3}$), lNACW (26.7 kg·m$^{-3}$<$\sigma_0$<27.2 kg·m$^{-3}$), AAIW (27.2 kg·m$^{-3}$<$\sigma_0$<27.6 kg·m$^{-3}$), uNADW ($\sigma_0$>27.6 kg·m$^{-3}$ and $\sigma_2$<37 kg·m$^{-3}$), lNADW ($\sigma_2$>37 kg·m$^{-3}$ and $\sigma_4$<45.9 kg·m$^{-3}$) and AABW ($\sigma_4$>45.9 kg·m$^{-3}$).

**Figure 2.** Mean distributions of $C_{ant}^{\varphi C_T^0}$ (µmol·kg$^{-1}$) along the A05 section for the eastern (right panel) and western (left panel) subtropical North Atlantic basins, in 1992 (red line) and 2011 (blue line). The respective shaded areas correspond to the standard deviation of the mean $C_{ant}^{\varphi C_T^0}$ estimates.

**Figure 3**. Averaged $C_{ant}$ concentrations (µmol·kg$^{-1}$) within each box and its uncertainty indicated by the coloured dots and the corresponding error bars (double of std): [$C_{ant}^{\varphi C_T^0}$] (red), [$C_{ant}^{TrOCA}$] (blue), [$C_{ant}^{\Delta C^*}$] (green), [$C_{ant}^{TTD}$] (grey). The associated coloured lines are the respective DT (µmol·kg$^{-1}$·yr$^{-1}$). Each horizontal panel corresponds to each layer, which are divided in subpanels identifying the regions. Mean TSSR ± standard deviation is indicated in each box as the area between purple dotted lines. Note that the scale in the y-axes is different depending on the layer, in order to help distinguishing the change in $C_{ant}$ between cruises; the total range of the y-axis spans 45 µmolkg$^{-1}$ for uNACW and INACW, 40 µmolkg$^{-1}$ for AAIW and uNADW, and 20 µmolkg$^{-1}$ for lNADW and AABW.

**Figure 4.** $C_{ant}$ storage rates (µmol·kg$^{-1}$ yr$^{-1}$), with their uncertainty. The storage rates calculated trough the DT (coloured circles) or the TSSR (coloured crosses) approaches, by using each method: ΔC* (green), $\varphi C_T^0$ (red), TrOCA (blue) and TTD (grey). Mean values, considering the four methods, through the DT (pink) and the TSSR (purple) approaches are also shown. Each horizontal panel corresponds to each layer, which are divided in subpanels identifying the regions. The yellow dashed-dotted line indicates

the average DT along each whole layer, summing up the regions. Vertical thicker lines highlight the boundary between the Florida Strait and the main section and that between the western and the eastern basins along the Mid-Atlantic Ridge. The corresponding values are reported in Table C1, in Appendix C. Note that the scale in the y-axis is different depending on the layer, in order to help distinguishing the values of the storage rates between methods. The total range of the y-axis spans 1 $\mu molkg^{-}1 \cdot y^{-1}$ for uNACW, lNACW and AAIW panels, and 0. 7 $\mu molkg^{-}1 \cdot y^{-1}$ for uNADW, lNADW and AABW.

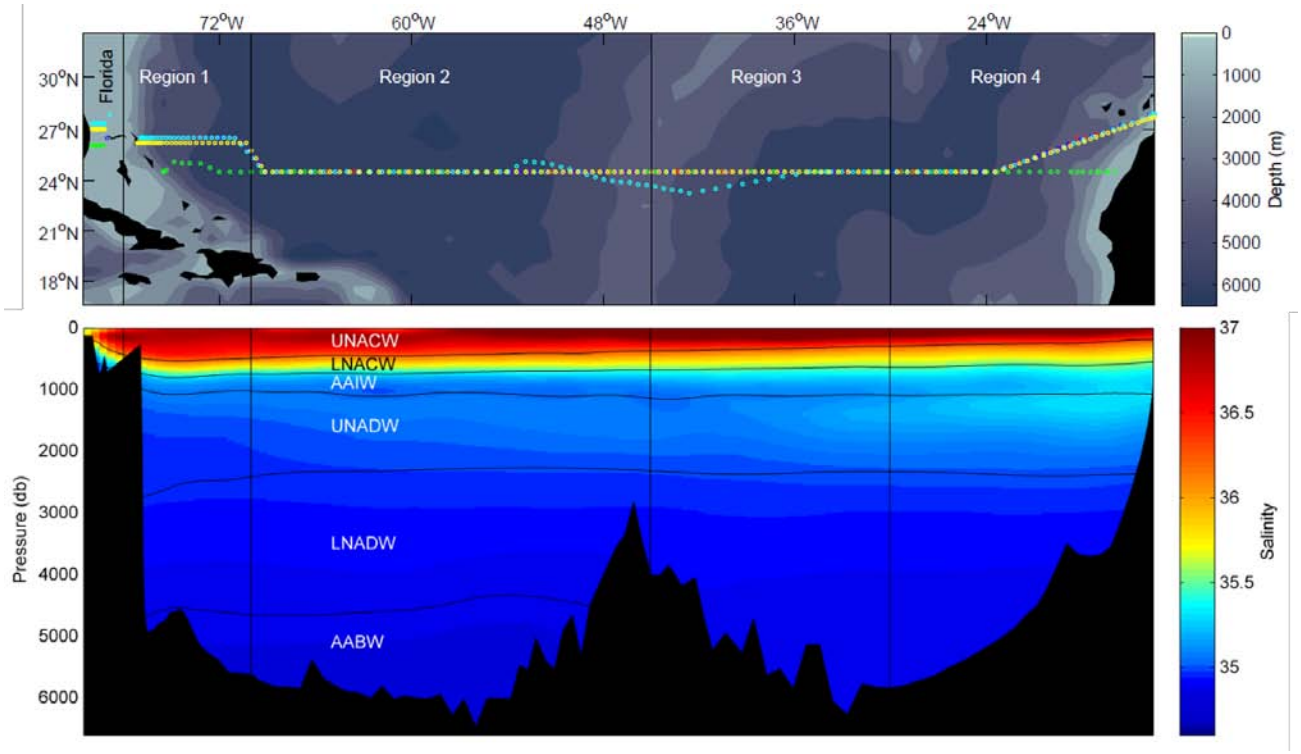
72°W
60°W
48°W
36°W
24°W
30°N
27°N
24°N
21°N
18°N
Florida
Region 1
Region 2
Region 3
Region 4
0
1000
2000
3000
4000
5000
6000
Depth (m)
Pressure (db)
UNACW
LNACW
AAIW
UNADW
LNADW
AABW
37
36.5
36
35.5
35
Salinity

Cant φCT°

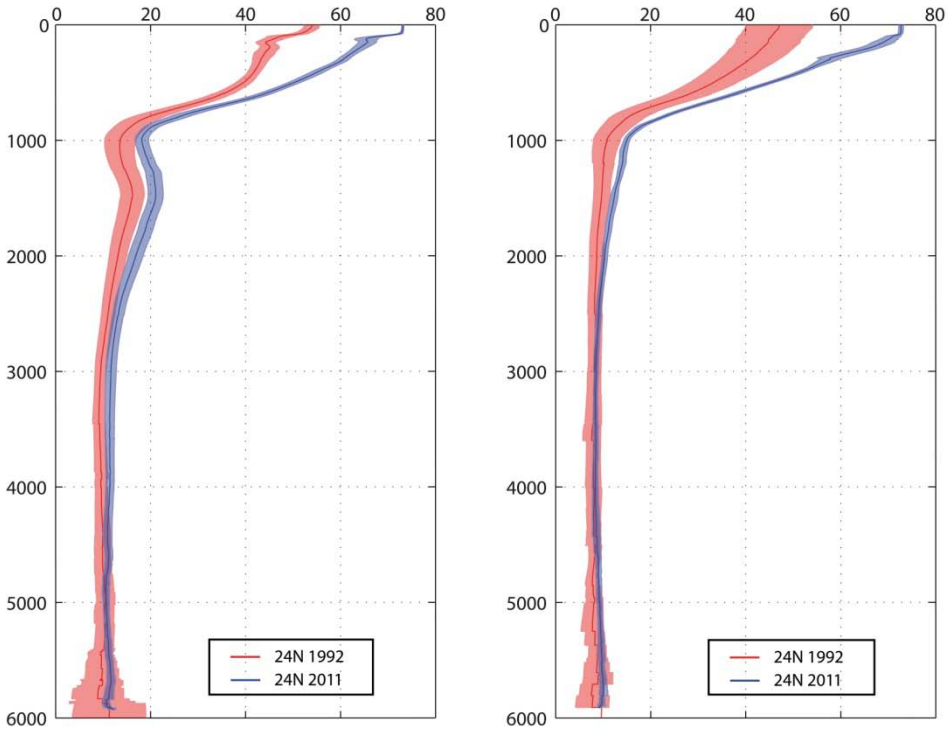
0
20
40
60
80
0
1000
2000
3000
4000
5000
6000
24N 1992
24N 2011
0
20
40
60
80
0
1000
2000
3000
4000
5000
6000
24N 1992
24N 2011

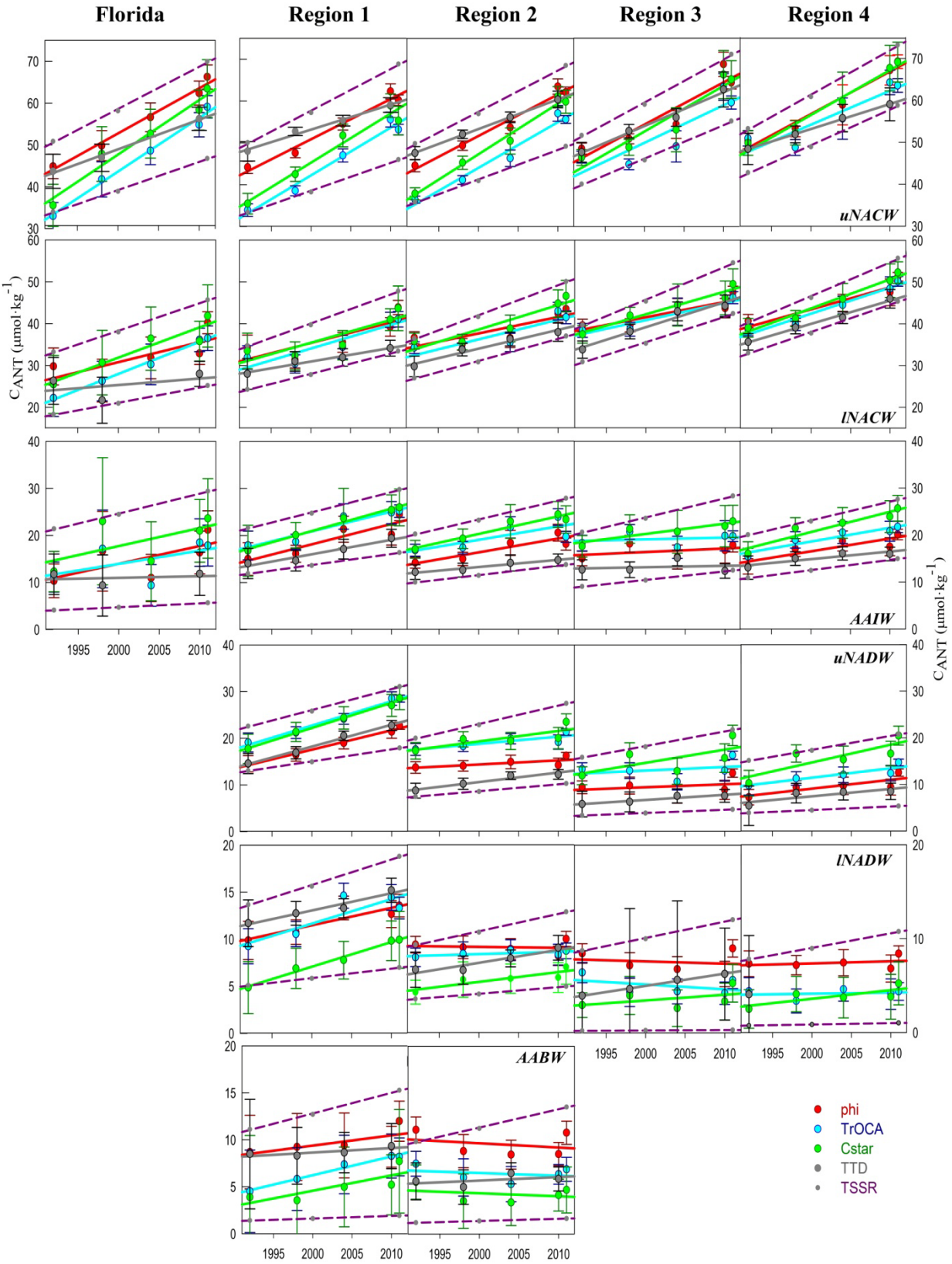
Florida
Region 1
Region 2
Region 3
Region 4
uNACW
lNACW
AAIW
uNADW
lNADW
AABW
C_ANT (µmol·kg⁻¹)
C_ANT (µmol·kg⁻¹)
1995
2000
2005
2010
phi
TrOCA
Cstar
TTD
TSSR

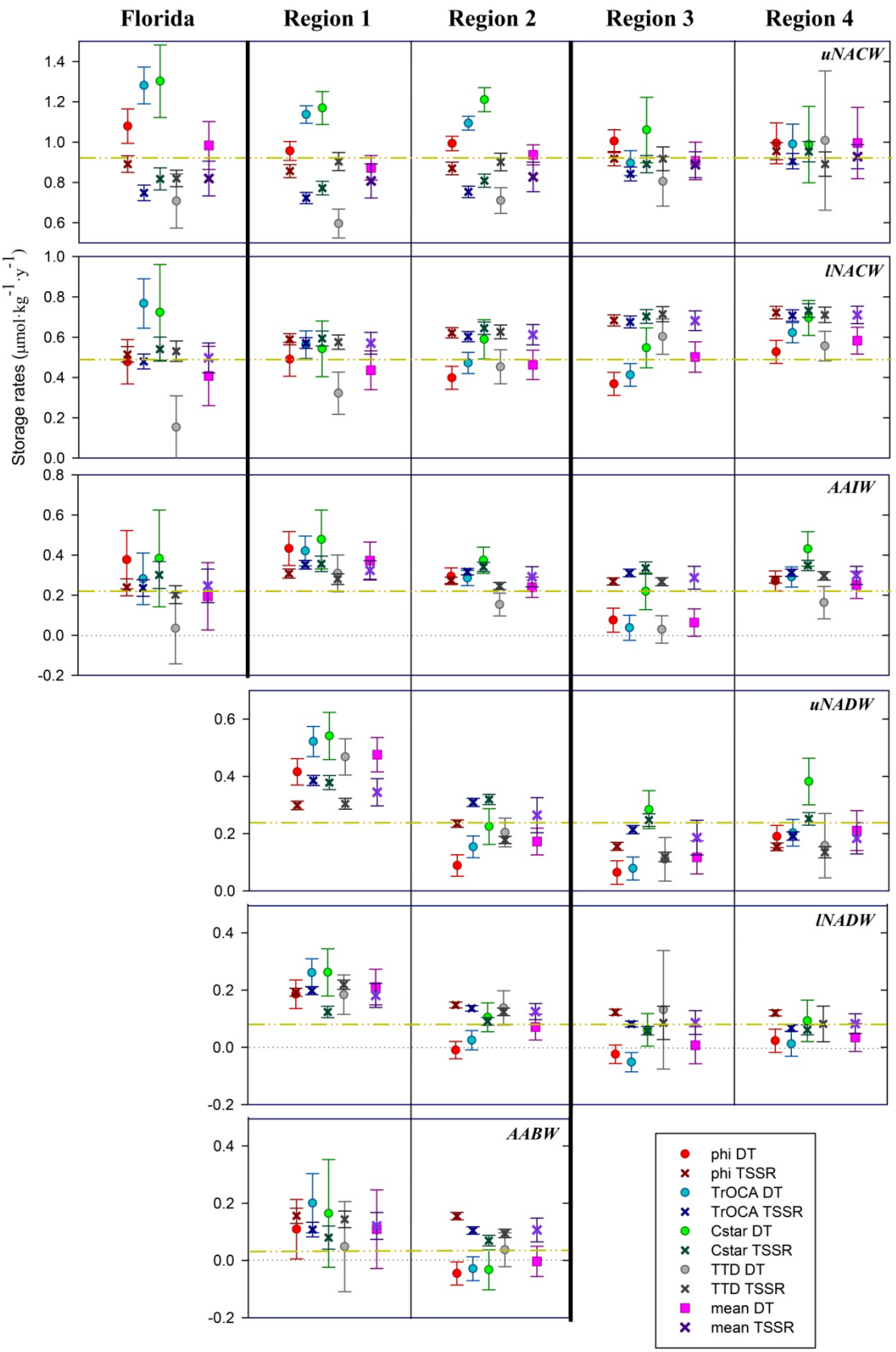
Florida
Region 1
Region 2
Region 3
Region 4
uNACW
lNACW
AAIW
uNADW
lNADW
AABW
Storage rates (µmol·kg-1·y-1)
phi DT
phi TSSR
TrOCA DT
TrOCA TSSR
Cstar DT
Cstar TSSR
TTD DT
TTD TSSR
mean DT
mean TSSR

# Supplementary information

**CONTENTS**



## A. Anthropogenic $CO_2$ computations.

We used three back-calculation methods to estimate anthropogenic $CO_2$ ($C_{ant}$) from in situ measurements. The principles of the carbon-based methods were established by Brewer (1978) and Chen and Millero (1979) and rely on separating the contributions to dissolved inorganic carbon ($C_T$) of organic matter remineralization and $CaCO_3$ dissolution, according to Redfield equations. In addition, the preindustrial preformed $C_T$ ($CT^0$, i.e. the $C_T$ that the water mass had at the moment of its formation in the preindustrial atmosphere) is also removed, taking the remaining $C_T$ amount as the $C_{ant}$ perturbation. The classical $\Delta C^*$ approach (Gruber et al., 1996) is a widely applied technique based on the estimation of the quasi-conservative $\Delta C^*$ tracer. This method first introduced the time-independent $\Delta C_{dis}$ term to the back-calculation techniques, under the assumption that it has remained steady since the preindustrial era. The authors proposed the $\Delta C_{dis}$ as one of the two terms in which they separated the $C_T^0$, together with a zero-$C_{ant}$ reference term that can be estimated according to the $CO_2$ system chemistry. The authors proposed a formal way to estimate the $\Delta C_{dis}$ through the use of age tracers, according to which old water masses are assumed to be void of $C_{ant}$ and $\Delta C_{dis}$ is assigned the value of $\Delta C^*$. For younger water masses $\Delta C_{dis}$ is calculated according to water age information. The uncertainties of the $\Delta C^*$ method were evaluated at ±9 $\mu mol \cdot kg^{-1}$ (Gruber et al., 1996). This error was evaluated assuming a lower precision for both $C_T$ and total alkalinity data than the obtained using modern and

standardized methods of analysis. For modern measurements the $C_{ant}^{\Delta C^*}$ error would thus be lower (Gruber, 1998) and closer to the uncertainty reported for other methods of estimation (around ±6 µmol·kg$^{-1}$).

The $\varphi C_T^0$ method (Vázquez-Rodríguez et al., 2009a) shares similar principles with $\Delta C^*$. It proposes some upgrades to the $\Delta C_{dis}$ and the preformed $A_T$ ($A_T^0$) determinations by using the subsurface layer (100-200m) as a reference for characterising water mass properties at their wintertime formation conditions. It thus avoids the short-term variability of the uppermost layers (Vázquez-Rodríguez et al., 2012). One important point in this approach is that none of the $A_T^0$ or $\Delta C_{dis}$ parametrizations rely on CFC data but on conservative parameters exclusively. Both terms are further assumed not to be in steady state. To address the assumption of invariable $\Delta C_{dis}$ (Matsumoto and Gruber, 2005), the $\varphi C_T^0$ method proposes an approximation to the spatial and temporal variability of $\Delta C_{dis}$ ($\Delta\Delta C_{dis}$) (Vázquez-Rodríguez et al., 2009a). It also accounts for the small increase of $A_T^0$ since the Industrial era due to $CaCO_3$ dissolution changes projected from models (Heinze, 2004) and the effect of rising sea surface temperatures on $A_T^0$. The $C_{ant}^{\varphi C_T^0}$ concentrations are directly estimated in waters above the 5ºC isotherm while they are estimated by using an extended Optimum MultiParameter (eOMP) analysis in waters with $\Theta < 5$ºC, improving the estimations in cold deep waters. An uncertainty of ±5.2 µmol·kg$^{-1}$ is obtained for $C_{ant}^{\varphi C_T^0}$ estimations (Vázquez-Rodríguez et al., 2009a).

The TrOCA method (Touratier and Goyet, 2004; Touratier et al., 2007) is an easy-to-apply technique based on the universal quasi-conservative TrOCA tracer (Tracer combining Oxygen, $C_T$ and $A_T$). It shares with the above methods its consideration of the biological contribution to $C_T$ but does not take into account the $C_T^0$ estimation in its parameterization. The $C_{ant}^{TrOCA}$ concentration is estimated from the difference between TrOCA and the preindustrial zero-$C_{ant}$ term $TrOCA^0$, defined from the "natural" concentrations of $O_2$, $C_T$ and $A_T$. The universal $TrOCA^0$ equation is a function of $\Theta$ and $A_T$, and was derived from $\Delta^{14}C$ and CFC-11 tracer data in the global ocean, to establish which water parcels can be assumed to be free of $C_{ant}$. The method assumes that $A_T$ is not affected by the increase of atmospheric $CO_2$ (Goyet et al., 1999) and uses a constant oxygen to carbon Redfield ratio (Rc) value of 1.35 (after Körtzinger et al., (1998)) to calculate the biological contribution to $C_T$, while both $\varphi C_T^0$ and $\Delta C^*$ methods use the

Rc ratio of 1.45 proposed by Anderson and Sarmiento (1994). Despite being a simple universal equation (Yool et al., 2010), it provides comparable $C_{ant}$ inventories to those obtained by other approaches in the Atlantic (Vázquez-Rodríguez et al., 2009b). The reported uncertainty for $C_{ant}^{TrOCA}$ estimations is ±6.25 µmol·kg$^{-1}$ (Touratier et al., 2007).

Given the availability of CFC measurements on four cruises (1992, 1998, 2004 and 2010), $C_{ant}$ concentrations were also estimated using the TTD method (Waugh et al., 2006), without using $CO_2$ measurements. Similar to all tracer-based methods, it aims to mathematically describe the Transit Time Distributions (TTD) of the CFCobservations to "calibrate" how the ocean's circulation connects surface boundary conditions with interior ocean concentrations. To estimate the ocean interior $C_{ant}^{TTD}$ at any given point of space and time, the only necessary information is the knowledge about the temporal evolution of $C_{ant}$ in the surface mixed layer and the rate at which this surface boundary condition is transported and mixed into the ocean interior. The assumption of the transport is steady and TTDs are modelled as Inverse Gaussian functions (Waugh et al., 2004). A constant air–sea disequilibrium in time is also assumed. Thus, $C_{ant}^{TTD}$ is the difference between $C_T$ at the time when the measurements were done, and $C_T$ just in the beginning of the preindustrial era (Waugh et al., 2004). The reported uncertainties of the TTD approach are ±6 µmol·kg$^{-1}$ (Waugh et al., 2006). CFC-12 was used as a proxy for $C_{ant}$ to constrain the TTD functions in each cruise (with a ratio of 1 for the mean and width of the TTD). The atmospheric histories for CFC-12 in the northern hemisphere are from John Bullister at CDIAC (http://cdiac.ornl.gov/oceans/new_atmCFC.html) and the $CO_2$ are from ftp://ftp.cmdl.noaa.gov. CFC-12 partial pressures at interior locations were calculated from its dissolved measured concentration using the solubility functions determined by Warner and Weiss (1985) with a time-invariant initial saturation at 100% for mode waters, at 85% for intermediate waters and at 65% for deep and bottom waters. We only used CFC-12 for consistency between cruises as this tracer was available for the 4 cruises (SF6 was only measured during the 2010 cruise) but this is problematic for the recently ventilated waters (uppermost water layers here) surveyed after the mid-1990's because of the decrease of atmospheric CFC-12 since then. The exclusion of data above 150 dbar from our estimates should help with this issue, and no correction was done by using any other tracer (such as SF6) to adjust results for younger waters or for change of saturation of the CFC-12 overtime (Tanhua et al., 2008). However, we took these issues into account in the interpretation section.

## References


Anderson, L.A., Sarmiento, J.L., 1994. Redfield ratios of remineralization determined by nutrient data analysis. Global Biogeochemical Cycles, 8, 65-80.

Brewer, P.G., 1978. Direct observation of the oceanic CO2 increase. Geophysical Research Letters, 5, 997-1000.

Chen, G.T., Millero, F.J., 1979. Gradual increase of oceanic CO2. Nature, 277, 205-206.

Goyet, C., Coatanoan, C., Eischeid, G., Amaoka, T., Okuda, K., Healy, R., Tsunogai, S., 1999. Spatial variation of total $CO_2$ and total alkalinity in the northern Indian Ocean: A novel approach for the quantification of anthropogenic $CO_2$ in seawater. Journal of Marine Research, 57, 135-163.

Gruber, N., 1998. Anthropogenic $CO_2$ in the Atlantic Ocean. Global Biogeochemical Cycles, 12, 165-191.

Gruber, N., Sarmiento, J.L., Stocker, T.F., 1996. An improved method for detecting anthropogenic CO2 in the oceans. Global Biogeochemical Cycles, 10, 809-837.

Körtzinger, A., Mintrop, L., Duinker, J.C., 1998. On the penetration of anthropogenic CO2 into the North Atlantic Ocean. Journal of Geophysical Research: Oceans, 103, 18681-18689.

Tanhua, T., Waugh, D.W., Wallace, D.W.R., 2008. Use of SF6 to estimate anthropogenic CO2 in the upper ocean. Journal of Geophysical Research C: Oceans, 113.

Touratier, F., Azouzi, L., Goyet, C., 2007. CFC-11, Δ14C and 3H tracers as a means to assess anthropogenic CO2 concentrations in the ocean. Tellus, Series B: Chemical and Physical Meteorology, 59, 318-325.

Touratier, F., Goyet, C., 2004. Definition, properties, and Atlantic Ocean distribution of the new tracer TrOCA. Journal of Marine Systems, 46, 169-179.

Vázquez-Rodríguez, M., Padin, X.A., Pardo, P.C., Ríos, A.F., Pérez, F.F., 2012. The subsurface layer reference to calculate preformed alkalinity and air–sea CO2 disequilibrium in the Atlantic Ocean. Journal of Marine Systems, 94, 52-63.

Vázquez-Rodríguez, M., Padin, X.A., Ríos, A.F., Bellerby, R.G.J., Pérez, F.F., 2009. An upgraded carbon-based method to estimate the anthropogenic fraction of dissolved CO2 in the Atlantic Ocean. Biogeosciences Discuss., 6, 4527.

Warner, M.J., Weiss, R.F., 1985. Solubilities of chlorofluorocarbons 11 and 12 in water and seawater. Deep Sea Research Part A. Oceanographic Research Papers, 32, 1485-1497.

Waugh, D.W., Haine, T.W.N., Hall, T.M., 2004. Transport times and anthropogenic carbon in the subpolar North Atlantic Ocean. Deep-Sea Research Part I: Oceanographic Research Papers, 51, 1475-1491.

Waugh, D.W., Hall, T.M., McNeil, B.I., Key, R., Matear, R.J., 2006. Anthropogenic CO2 in the oceans estimated using transit time distributions. Tellus, Series B: Chemical and Physical Meteorology, 58, 376-389.

Yool, A., Oschlies, A., Nurser, A.J.G., Gruber, N., 2010. A model-based assessment of the TrOCA approach for estimating anthropogenic carbon in the ocean. Biogeosciences, 7, 723-751.

## Appendix B. Box-averaged physico-chemical properties and $C_{ant}$ estimations

The tables in this appendix summarize mean values ± standard error of the mean ($x \pm \sigma/\sqrt{N}$) for pressure (dbar), salinity, $O_2$ ($\mu mol \cdot kg^{-1}$), potential temperature Θ (ºC) Apparent Oxygen Utilization (AOU, $\mu mol \cdot kg^{-1}$) within each given layer and region box. Regarding the $C_{ant}$ estimations, tables summarize mean $C_{ant}$ ± standard deviation of an ensemble of 100 $C_{ant}$ averages computed by random perturbations of the $C_{ant}$ estimates within each given box according to each method uncertainty.

**Supplementary Table B1.** Physico-chemical properties and $C_{ant}$ estimations in Region 1 (78°W to 70°W).

| | Press (dbar) | salinity | Θ (ºC) | AOU (µmol/kg) | $\varphi C_T^0$ (µmol/kg) | TrOCA (µmol/kg) | ΔC* (µmol/kg) | TTD (µmol/kg) |
|---|---|---|---|---|---|---|---|---|
| **1 REGION** | | | | | | | | |
| **uNACW** | | | | | | | | |
| 1992 | 268.3±14.0 | 36.627±0.021 | 19.49±0.24 | 29.7±1.9 | 44.1±0.7 | 33.9±0.7 | 35.5±1.2 | 48.0±1.2 |
| 1998 | 310.7±6.4 | 36.578±0.010 | 18.60±0.08 | 33.1±0.7 | 47.6±0.6 | 38.6±0.6 | 42.5±0.9 | 52.8±0.5 |
| 2004 | 355.8±10.9 | 36.556±0.017 | 18.61±0.15 | 37.9±1.5 | 54.5±0.7 | 47.0±0.8 | 51.8±1.4 | 55.3±0.6 |
| 2010 | 321.7±11.5 | 36.552±0.017 | 18.51±0.14 | 36.1±1.2 | 62.3±0.9 | 55.6±0.9 | 58.9±1.4 | 59.1±0.9 |
| 2011 | 279.7±9.7 | 36.611±0.014 | 18.89±0.14 | 30.8±1.3 | 60.2±0.6 | 53.2±0.6 | 55.3±1.7 | |
| **lNACW** | | | | | | | | |
| 1992 | 630.0±22.5 | 35.768±0.061 | 13.19±0.42 | 89.7±5.4 | 34.3±1.5 | 31.9±1.4 | 33.5±2.1 | 28.0±1.8 |
| 1998 | 666.4±8.5 | 35.748±0.025 | 13.08±0.17 | 92.6±1.9 | 31.3±1.0 | 30.4±1.1 | 32.3±1.7 | 31.0±1.2 |
| 2004 | 714.1±10.4 | 35.632±0.031 | 12.32±0.23 | 103.5±3.5 | 35.5±1.2 | 34.4±1.4 | 34.9±1.8 | 31.9±1.0 |
| 2010 | 678.1±10.1 | 35.664±0.030 | 12.57±0.21 | 101.0±2.6 | 39.2±1.1 | 40.9±0.9 | 41.0±1.3 | 34.1±0.9 |
| 2011 | 642.7±12.2 | 35.718±0.032 | 12.98±0.23 | 100.8±2.4 | 43.9±0.8 | 41.1±0.9 | 43.7±2.7 | |
| **AAIW** | | | | | | | | |
| 1992 | 887.9±27.0 | 35.158±0.021 | 7.99±0.30 | 124.8±2.3 | 15.0±1.7 | 17.9±1.5 | 16.8±2.7 | 14.1±1.6 |
| 1998 | 926.2±9.5 | 35.160±0.010 | 8.07±0.13 | 126.5±0.9 | 16.1±0.9 | 18.7±0.8 | 20.1±1.3 | 14.7±1.1 |
| 2004 | 923.8±12.8 | 35.149±0.012 | 7.98±0.16 | 125.7±1.9 | 21.4±1.4 | 24.1±1.4 | 23.7±3.2 | 17.1±1.0 |
| 2010 | 921.5±10.7 | 35.150±0.009 | 7.89±0.14 | 121.9±1.5 | 20.2±1.1 | 24.9±1.2 | 25.4±1.6 | 19.4±1.0 |
| 2011 | 899.3±8.6 | 35.137±0.007 | 7.76±0.11 | 124.8±1.3 | 24.4±0.6 | 25.2±0.7 | 26.0±2.0 | |
| **uNADW** | | | | | | | | |
| 1992 | 1,741.5±67.5 | 35.003±0.005 | 3.98±0.12 | 62.0±1.7 | 14.5±0.9 | 19.1±1.0 | 17.7±1.6 | 14.6±1.1 |
| 1998 | 1,787.1±29.1 | 35.000±0.003 | 4.00±0.05 | 60.9±0.8 | 16.4±0.7 | 21.2±0.6 | 21.4±1.0 | 16.9±0.7 |
| 2004 | 1,735.8±37.0 | 34.997±0.004 | 4.06±0.07 | 63.3±1.1 | 19.0±0.6 | 24.2±0.6 | 24.4±1.2 | 20.5±0.5 |
| 2010 | 1,821.3±34.9 | 34.985±0.003 | 3.84±0.06 | 56.0±0.7 | 21.4±0.7 | 28.5±0.7 | 27.0±1.2 | 22.7±0.5 |
| 2011 | 1,596.3±29.3 | 35.005±0.003 | 4.27±0.06 | 65.3±0.8 | 22.7±0.4 | 28.5±0.4 | 28.6±1.2 | |
| **lNADW** | | | | | | | | |
| 1992 | 3,779.6±111.3 | 34.913±0.003 | 2.19±0.05 | 62.3±0.5 | 9.9±1.0 | 9.2±0.9 | 4.9±1.4 | 11.7±1.2 |
| 1998 | 3,533.1±43.3 | 34.916±0.001 | 2.27±0.02 | 59.4±0.2 | 10.8±0.6 | 10.5±0.7 | 6.9±1.1 | 12.7±0.6 |
| 2004 | 3,626.7±46.9 | 34.910±0.001 | 2.19±0.02 | 63.2±0.3 | 13.3±0.6 | 14.6±0.7 | 7.8±1.0 | 13.3±0.5 |
| 2010 | 3,540.3±60.0 | 34.910±0.002 | 2.23±0.03 | 58.1±0.3 | 12.7±0.7 | 14.4±0.7 | 9.8±1.1 | 15.2±0.6 |
| 2011 | 3,726.8±56.8 | 34.908±0.002 | 2.17±0.03 | 63.2±0.3 | 13.6±0.6 | 13.3±0.6 | 9.9±1.5 | |
| **AABW** | | | | | | | | |
| 1992 | 5,406.6±107.9 | 34.865±0.004 | 1.67±0.03 | 78.8±1.7 | 8.7±2.0 | 4.5±2.2 | 3.9±3.3 | 8.5±2.9 |
| 1998 | 5,042.7±58.8 | 34.871±0.002 | 1.71±0.02 | 75.0±0.8 | 9.2±1.8 | 5.8±1.7 | 3.5±2.5 | 8.3±1.5 |
| 2004 | 5,007.9±50.1 | 34.870±0.002 | 1.71±0.01 | 78.2±0.8 | 9.4±1.7 | 7.4±1.6 | 5.0±2.1 | 8.6±1.1 |
| 2010 | 4,939.6±60.9 | 34.961±0.049 | 1.72±0.01 | 72.5±5.8 | 9.3±1.1 | 8.3±1.2 | 5.2±1.6 | 9.3±1.2 |
| 2011 | 5,031.8±60.0 | 34.871±0.002 | 1.71±0.01 | 77.0±0.9 | 12.0±1.1 | 8.2±1.0 | 7.7±2.8 | |

**Supplementary Table B2.** Physico-chemical properties and $C_{ant}$ estimations in Region 2 (70°W to 45°W).

| | Press (dbar) | salinity | Θ (°C) | AOU (µmol/kg) | $\varphi C_T^0$ (µmol/kg) | TrOCA (µmol/kg) | ΔC* (µmol/kg) | TTD (µmol/kg) |
|---|---|---|---|---|---|---|---|---|
| **2 REGION** | | | | | | | | |
| **uNACW** | | | | | | | | |
| 1992 | 252.9±6.5 | 36.618±0.017 | 18.71±0.12 | 33.4±0.9 | 44.5±0.5 | 36.4±0.4 | 37.8±0.7 | 47.5±0.8 |
| 1998 | 277.9±4.7 | 36.569±0.011 | 18.26±0.07 | 35.0±0.6 | 49.3±0.5 | 41.1±0.5 | 45.3±0.8 | 52.0±0.5 |
| 2004 | 299.3±10.2 | 36.514±0.020 | 18.05±0.14 | 38.9±1.4 | 53.7±1.1 | 46.3±1.0 | 50.5±1.6 | 56.1±0.6 |
| 2010 | 271.5±8.2 | 36.574±0.022 | 18.37±0.13 | 39.3±1.2 | 63.5±0.9 | 57.1±0.9 | 61.1±1.2 | 60.4±1.0 |
| 2011 | 272.7±8.5 | 36.580±0.019 | 18.41±0.14 | 38.0±1.0 | 62.1±0.5 | 55.6±0.5 | 59.9±1.4 | |
| **lNACW** | | | | | | | | |
| 1992 | 562.3±9.9 | 35.823±0.024 | 13.37±0.17 | 79.0±2.0 | 36.6±0.7 | 34.2±0.7 | 35.8±1.0 | 29.7±1.2 |
| 1998 | 562.1±7.7 | 35.822±0.019 | 13.46±0.13 | 84.4±1.5 | 35.0±0.7 | 33.8±0.8 | 35.6±0.9 | 33.7±0.8 |
| 2004 | 600.8±12.7 | 35.739±0.035 | 12.89±0.25 | 91.9±3.1 | 36.5±1.1 | 35.5±1.1 | 38.8±1.6 | 36.3±0.8 |
| 2010 | 563.1±10.1 | 35.776±0.027 | 13.25±0.18 | 92.7±2.3 | 42.4±1.0 | 43.0±1.1 | 44.8±1.6 | 37.9±1.1 |
| 2011 | 574.9±10.4 | 35.752±0.025 | 13.06±0.17 | 94.7±2.1 | 43.5±0.8 | 41.5±0.8 | 46.6±1.9 | |
| **AAIW** | | | | | | | | |
| 1992 | 899.1±11.9 | 35.165±0.014 | 7.87±0.15 | 129.6±0.9 | 14.2±0.6 | 16.8±0.6 | 17.0±0.9 | 12.1±0.8 |
| 1998 | 899.9±8.6 | 35.149±0.010 | 7.91±0.10 | 130.4±0.7 | 15.0±0.7 | 17.3±0.7 | 19.2±1.0 | 12.6±0.7 |
| 2004 | 897.6±14.3 | 35.152±0.018 | 7.82±0.17 | 127.1±1.7 | 18.4±1.3 | 21.7±1.1 | 22.9±1.8 | 14.1±0.9 |
| 2010 | 882.9±9.9 | 35.149±0.013 | 8.05±0.13 | 134.1±1.1 | 20.5±0.9 | 23.9±0.9 | 24.4±1.4 | 14.7±0.6 |
| 2011 | 914.2±9.4 | 35.110±0.008 | 7.49±0.11 | 131.4±0.9 | 18.1±0.6 | 19.7±0.6 | 23.3±1.4 | |
| **uNADW** | | | | | | | | |
| 1992 | 1,672.1±27.5 | 35.046±0.003 | 4.26±0.06 | 72.9±1.0 | 13.7±0.6 | 17.5±0.6 | 17.3±0.9 | 8.7±0.8 |
| 1998 | 1,690.8±22.0 | 35.035±0.002 | 4.25±0.05 | 72.4±0.9 | 14.0±0.6 | 18.3±0.6 | 19.7±0.8 | 10.2±0.6 |
| 2004 | 1,652.7±25.9 | 35.034±0.002 | 4.29±0.06 | 73.6±1.1 | 14.9±0.7 | 19.9±0.6 | 19.4±0.9 | 11.9±0.4 |
| 2010 | 1,767.1±26.5 | 35.028±0.005 | 4.14±0.06 | 72.3±1.0 | 14.2±0.8 | 19.1±0.8 | 20.0±1.1 | 12.2±0.5 |
| 2011 | 1,536.7±19.5 | 35.044±0.002 | 4.53±0.05 | 76.7±0.9 | 16.2±0.4 | 21.3±0.4 | 23.4±0.9 | |
| **lNADW** | | | | | | | | |
| 1992 | 3,421.9±51.6 | 34.922±0.002 | 2.32±0.03 | 70.6±0.4 | 9.4±0.4 | 8.0±0.5 | 4.3±0.6 | 6.7±0.9 |
| 1998 | 3,314.0±38.6 | 34.925±0.002 | 2.38±0.02 | 69.0±0.3 | 9.1±0.6 | 8.4±0.6 | 5.6±0.9 | 6.6±0.8 |
| 2004 | 3,398.9±41.2 | 34.921±0.002 | 2.32±0.02 | 69.4±0.3 | 8.9±0.6 | 8.8±0.6 | 5.7±0.8 | 7.9±0.4 |
| 2010 | 3,436.7±50.4 | 34.921±0.002 | 2.33±0.03 | 69.8±0.4 | 8.2±0.5 | 8.3±0.6 | 5.9±0.8 | 9.0±0.7 |
| 2011 | 3,403.2±46.9 | 34.921±0.002 | 2.32±0.03 | 71.5±0.3 | 10.0±0.4 | 8.7±0.4 | 7.0±0.9 | |
| **AABW** | | | | | | | | |
| 1992 | 5,279.1±65.3 | 34.858±0.002 | 1.59±0.02 | 82.1±0.5 | 11.1±0.7 | 7.5±0.7 | 5.5±0.9 | 5.6±1.0 |
| 1998 | 5,302.8±47.2 | 34.856±0.001 | 1.60±0.01 | 79.9±0.4 | 8.8±0.9 | 6.0±1.0 | 3.5±1.4 | 5.0±0.9 |
| 2004 | 5,313.0±37.6 | 34.857±0.001 | 1.60±0.01 | 80.9±0.5 | 8.4±0.8 | 5.3±0.9 | 3.4±1.2 | 6.5±0.6 |
| 2010 | 5,473.9±69.5 | 34.886±0.016 | 1.66±0.04 | 81.5±0.6 | 8.5±0.6 | 6.4±0.5 | 4.1±0.8 | 5.9±0.6 |
| 2011 | 5,300.6±44.0 | 34.858±0.001 | 1.61±0.01 | 83.2±0.4 | 10.8±0.6 | 6.9±0.6 | 4.7±1.2 | |

**Supplementary Table B3.** Physico-chemical properties and $C_{ant}$ estimations in Region 3 (45°W to 30°W).

| | Press (dbar) | salinity | Θ (ºC) | AOU (µmol/kg) | $\varphi C_T^0$ (µmol/kg) | TrOCA (µmol/kg) | ΔC* (µmol/kg) | TTD (µmol/kg) |
|---|---|---|---|---|---|---|---|---|
| **3 REGION** | | | | | | | | |
| **uNACW** | | | | | | | | |
| 1992 | 220.0±6.5 | 36.656±0.033 | 18.30±0.17 | 32.9±1.5 | 48.6±0.7 | 46.6±0.7 | 46.5±0.9 | 47.8±1.2 |
| 1998 | 248.3±4.9 | 36.588±0.020 | 18.02±0.11 | 34.3±0.9 | 51.0±0.6 | 44.9±0.6 | 48.9±1.0 | 52.8±0.8 |
| 2004 | 259.2±13.5 | 36.497±0.040 | 17.76±0.24 | 38.7±1.6 | 54.4±1.7 | 49.2±1.9 | 53.1±2.6 | 56.0±1.0 |
| 2010 | 220.1±7.4 | 36.724±0.039 | 18.67±0.19 | 35.2±1.5 | 68.8±1.5 | 63.4±1.6 | 66.3±2.9 | 62.8±2.1 |
| 2011 | 219.9±8.7 | 36.676±0.036 | 18.63±0.21 | 34.8±1.6 | 64.4±0.8 | 59.6±0.8 | 65.2±2.2 | |
| **lNACW** | | | | | | | | |
| 1992 | 489.0±11.6 | 35.807±0.023 | 13.20±0.17 | 74.8±2.1 | 39.5±0.7 | 38.3±0.8 | 37.4±1.1 | 33.7±1.0 |
| 1998 | 501.8±9.4 | 35.865±0.022 | 13.53±0.15 | 73.6±1.8 | 39.6±0.8 | 38.6±0.8 | 41.9±1.0 | 38.1±0.9 |
| 2004 | 474.0±15.9 | 35.879±0.031 | 13.77±0.23 | 77.4±2.9 | 42.8±1.6 | 42.8±1.7 | 44.4±2.5 | 42.9±1.1 |
| 2010 | 489.9±13.5 | 35.840±0.033 | 13.42±0.23 | 84.1±2.9 | 43.7±1.2 | 44.2±1.3 | 46.1±2.0 | 44.2±1.3 |
| 2011 | 488.7±13.4 | 35.850±0.030 | 13.47±0.21 | 81.6±2.6 | 47.5±0.7 | 46.2±0.7 | 49.4±1.8 | |
| **AAIW** | | | | | | | | |
| 1992 | 875.4±15.7 | 35.250±0.016 | 8.22±0.17 | 132.2±1.2 | 15.1±0.8 | 18.3±0.8 | 17.7±1.1 | 12.7±1.1 |
| 1998 | 877.9±13.3 | 35.259±0.015 | 8.39±0.15 | 128.7±1.2 | 18.2±0.9 | 20.7±0.8 | 21.3±1.5 | 12.7±0.8 |
| 2004 | 877.6±22.4 | 35.245±0.023 | 8.32±0.24 | 129.3±1.5 | 15.4±1.3 | 17.4±1.2 | 20.8±2.3 | 15.2±0.8 |
| 2010 | 877.1±13.1 | 35.195±0.013 | 7.95±0.14 | 138.4±1.0 | 16.8±1.4 | 19.9±1.6 | 21.9±2.2 | 12.4±0.8 |
| 2011 | 922.3±10.8 | 35.172±0.009 | 7.64±0.10 | 135.2±0.6 | 17.9±0.7 | 19.8±0.6 | 23.0±1.7 | |
| **uNADW** | | | | | | | | |
| 1992 | 1,725.5±40.5 | 35.070±0.006 | 4.44±0.10 | 87.6±1.6 | 9.4±0.7 | 13.4±0.7 | 11.9±1.0 | 5.8±1.4 |
| 1998 | 1,717.4±30.1 | 35.063±0.004 | 4.47±0.07 | 87.0±1.2 | 9.8±0.9 | 13.0±0.9 | 16.5±1.2 | 6.3±1.1 |
| 2004 | 1,725.3±37.1 | 35.067±0.005 | 4.47±0.09 | 88.4±1.5 | 7.6±0.8 | 10.6±0.9 | 12.9±1.4 | 7.6±0.8 |
| 2010 | 1,733.1±34.7 | 35.061±0.006 | 4.42±0.08 | 89.1±1.4 | 8.9±1.0 | 13.0±1.1 | 15.7±1.5 | 7.6±0.7 |
| 2011 | 1,539.3±23.7 | 35.081±0.004 | 4.90±0.06 | 95.3±1.2 | 12.5±0.4 | 16.3±0.4 | 20.6±1.1 | |
| **lNADW** | | | | | | | | |
| 1992 | 3,788.6±87.6 | 34.921±0.003 | 2.32±0.03 | 81.6±0.2 | 8.5±0.5 | 6.4±0.5 | 3.0±0.7 | 4.0±2.4 |
| 1998 | 3,706.8±66.8 | 34.922±0.002 | 2.33±0.02 | 81.5±0.2 | 7.2±0.7 | 4.3±0.8 | 4.0±1.0 | 4.7±4.3 |
| 2004 | 3,891.3±70.9 | 34.916±0.002 | 2.26±0.02 | 81.6±0.3 | 6.8±0.7 | 4.4±0.7 | 2.6±1.0 | 5.6±4.2 |
| 2010 | 4,064.4±84.2 | 34.912±0.003 | 2.23±0.03 | 81.5±0.2 | 6.3±0.7 | 4.2±0.6 | 3.3±1.0 | 6.3±2.5 |
| 2011 | 3,919.6±71.0 | 34.916±0.002 | 2.26±0.03 | 83.9±0.2 | 9.0±0.5 | 5.6±0.4 | 5.3±1.0 | |

**Supplementary Table B4.** Physico-chemical properties and $C_{ant}$ estimations in Region 4 (30°W to 10°W).

| | Press (dbar) | salinity | Θ (°C) | AOU (µmol/kg) | $\varphi C_T^0$ (µmol/kg) | TrOCA (µmol/kg) | ΔC* (µmol/kg) | TTD (µmol/kg) |
|---|---|---|---|---|---|---|---|---|
| **4 REGION** | | | | | | | | |
| **uNACW** | | | | | | | | |
| 1992 | 182.7±5.0 | 36.630±0.033 | 17.78±0.15 | 33.1±2.4 | 50.3±0.9 | 51.0±0.9 | 49.8±1.5 | 48.4±1.9 |
| 1998 | 204.8±4.7 | 36.493±0.021 | 17.45±0.11 | 44.1±2.2 | 53.3±1.0 | 48.8±0.9 | 52.3±1.5 | 51.9±1.0 |
| 2004 | 213.7±5.6 | 36.420±0.037 | 17.18±0.19 | 46.0±3.1 | 58.9±2.4 | 55.7±2.5 | 59.7±3.5 | 55.8±1.6 |
| 2010 | 202.5±6.0 | 36.557±0.030 | 17.56±0.15 | 49.7±3.6 | 67.2±1.8 | 64.3±1.5 | 67.7±2.7 | 59.1±2.0 |
| 2011 | 165.4±4.0 | 36.522±0.020 | 17.77±0.13 | 43.5±2.4 | 69.3±0.8 | 63.6±0.8 | 69.2±2.4 | |
| **lNACW** | | | | | | | | |
| 1992 | 379.7±13.0 | 35.889±0.031 | 13.67±0.20 | 84.4±3.1 | 40.7±0.8 | 38.6±0.7 | 39.1±1.1 | 35.7±1.0 |
| 1998 | 396.9±8.3 | 35.869±0.016 | 13.45±0.11 | 84.5±1.7 | 40.8±0.6 | 39.8±0.7 | 41.3±1.0 | 39.1±0.7 |
| 2004 | 385.1±11.5 | 35.786±0.020 | 13.08±0.15 | 90.2±2.6 | 45.0±1.0 | 44.5±1.1 | 46.0±1.8 | 41.5±0.7 |
| 2010 | 413.3±13.8 | 35.865±0.029 | 13.45±0.19 | 87.2±3.2 | 47.5±1.6 | 48.4±1.4 | 50.3±2.0 | 46.0±1.1 |
| 2011 | 391.8±12.0 | 35.907±0.023 | 13.72±0.16 | 79.9±2.5 | 51.3±0.5 | 50.2±0.6 | 52.3±1.3 | |
| **AAIW** | | | | | | | | |
| 1992 | 812.0±19.1 | 35.235±0.015 | 8.38±0.16 | 155.0±1.9 | 13.3±0.8 | 15.4±0.9 | 16.0±1.3 | 13.1±1.2 |
| 1998 | 829.5±11.8 | 35.297±0.008 | 8.59±0.09 | 143.9±1.1 | 17.1±0.8 | 19.0±0.9 | 21.5±1.1 | 15.0±0.7 |
| 2004 | 820.1±17.5 | 35.276±0.013 | 8.51±0.14 | 147.0±1.5 | 18.7±1.1 | 20.5±1.2 | 22.6±1.6 | 16.1±0.7 |
| 2010 | 839.3±13.9 | 35.272±0.010 | 8.48±0.12 | 148.1±1.1 | 17.5±1.0 | 20.8±1.1 | 23.9±1.7 | 16.0±0.7 |
| 2011 | 874.6±11.8 | 35.279±0.008 | 8.29±0.09 | 144.2±0.9 | 20.1±0.6 | 21.7±0.6 | 25.7±1.4 | |
| **uNADW** | | | | | | | | |
| 1992 | 1,703.6±45.1 | 35.104±0.010 | 4.65±0.13 | 102.5±2.1 | 7.3±0.8 | 9.8±1.0 | 10.2±1.4 | 5.4±2.1 |
| 1998 | 1,678.4±28.2 | 35.151±0.007 | 5.00±0.09 | 102.5±1.0 | 9.4±0.7 | 11.3±0.7 | 16.6±0.9 | 8.1±1.1 |
| 2004 | 1,695.6±38.7 | 35.133±0.008 | 4.90±0.12 | 101.5±1.7 | 9.7±0.9 | 12.1±0.8 | 15.3±1.4 | 8.3±0.9 |
| 2010 | 1,764.6±31.5 | 35.130±0.008 | 4.70±0.10 | 98.6±1.0 | 9.4±0.9 | 12.4±0.8 | 16.6±1.3 | 8.5±0.9 |
| 2011 | 1,503.6±22.2 | 35.190±0.006 | 5.54±0.08 | 109.8±1.0 | 12.5±0.4 | 14.7±0.4 | 20.5±1.0 | |
| **lNADW** | | | | | | | | |
| 1992 | 3,701.4±103.5 | 34.923±0.004 | 2.33±0.04 | 84.7±0.5 | 7.3±0.7 | 4.4±0.7 | 2.5±1.0 | 4.1±3.1 |
| 1998 | 3,565.0±57.5 | 34.927±0.002 | 2.37±0.03 | 86.4±0.4 | 7.2±0.5 | 3.4±0.6 | 4.1±0.9 | |
| 2004 | 3,734.6±70.0 | 34.921±0.002 | 2.31±0.03 | 85.3±0.5 | 7.4±0.7 | 4.6±0.6 | 3.7±1.1 | |
| 2010 | 3,708.2±83.0 | 34.925±0.003 | 2.35±0.03 | 86.6±0.5 | 6.8±0.7 | 4.1±0.8 | 3.8±1.2 | |
| 2011 | 3,698.2±75.0 | 34.923±0.003 | 2.35±0.03 | 88.7±0.5 | 8.4±0.4 | 4.4±0.5 | 5.2±1.1 | |

**Supplementary Table B5.** Physico-chemical properties in Region 0 (Florida Strait, 80°W to 78°W).

| | Press (dbar) | salinity | Θ (ºC) | AOU (µmol/kg) | φ CT0 (µmol/kg) | TrOCA (µmol/kg) | ΔC* (µmol/kg) | TTD (µmol/kg) |
|---|---|---|---|---|---|---|---|---|
| **Florida** | | | | | | | | |
| **uNACW** | | | | | | | | |
| 1992 | 229.1±15.7 | 36.552±0.066 | 19.08±0.60 | 58.9±5.9 | 44.9±1.5 | 33.0±1.6 | 35.6±2.5 | 43.7±2.0 |
| 1998 | 250.7±10.8 | 36.514±0.037 | 18.78±0.32 | 69.6±2.6 | 49.8±1.8 | 41.8±2.1 | 47.8±3.3 | 46.9±1.6 |
| 2004 | 241.8±28.8 | 36.569±0.073 | 19.71±0.72 | 51.9±5.5 | 56.6±1.7 | 48.6±1.7 | 52.7±2.9 | |
| 2010 | 261.1±18.6 | 36.520±0.040 | 18.67±0.34 | 53.6±5.1 | 62.4±1.4 | 54.8±1.4 | 58.4±2.4 | 56.3±1.4 |
| 2011 | 228.1±14.5 | 36.543±0.042 | 18.89±0.37 | 63.9±3.1 | 66.3±1.4 | 59.1±1.3 | 63.5±3.5 | |
| **lNACW** | | | | | | | | |
| 1992 | 363.5±50.3 | 35.654±0.120 | 12.86±0.75 | 118.8±10.1 | 29.8±2.2 | 22.2±2.2 | 25.5±3.5 | 26.3±2.8 |
| 1998 | 380.3±22.9 | 35.508±0.051 | 12.02±0.34 | 135.3±3.0 | 26.4±2.6 | 26.3±2.4 | 30.7±3.9 | 21.7±2.7 |
| 2004 | 396.6±38.0 | 35.652±0.104 | 12.78±0.66 | 117.8±11.0 | 31.8±2.5 | 30.2±2.4 | 36.4±3.8 | |
| 2010 | 472.9±29.3 | 35.484±0.062 | 11.80±0.41 | 126.8±5.7 | 32.9±1.3 | 36.1±1.4 | 35.8±2.4 | 28.0±1.5 |
| 2011 | 399.6±34.3 | 35.435±0.065 | 11.47±0.44 | 135.4±4.4 | 40.2±1.3 | 36.5±1.5 | 41.8±3.7 | |
| **AAIW** | | | | | | | | |
| 1992 | 398.6±39.7 | 34.989±0.020 | 7.58±0.25 | 155.8±1.1 | 10.4±1.8 | 11.2±1.6 | 12.3±2.1 | 11.8±2.2 |
| 1998 | 561.8±31.7 | 34.951±0.017 | 7.24±0.27 | 157.9±1.4 | 16.7±4.2 | 17.2±4.1 | 23.0±6.8 | 9.4±3.3 |
| 2004 | 611.3±47.1 | 35.061±0.077 | 8.04±0.58 | 155.1±6.3 | 11.0±2.5 | 9.4±2.2 | 14.5±4.2 | |
| 2010 | 665.7±44.8 | 34.988±0.028 | 7.38±0.21 | 164.0±16.8 | 16.4±2.3 | 18.5±2.5 | 21.0±3.3 | 11.9±2.3 |
| 2011 | 545.0±49.7 | 34.940±0.012 | 7.10±0.20 | 158.9±0.7 | 21.2±2.0 | 17.9±2.2 | 23.6±4.2 | |

## Appendix C. $C_{ant}$ storage rates along the A05 section

The temporal changes in the mean $C_{ant}$ concentrations ([$C_{ant}$]) of $\varphi C_T^0$, TrOCA and $\Delta C^*$ ([$C_{ant}^{\varphi C_T^0}$], [$C_{ant}^{TrOCA}$], [$C_{ant}^{\Delta C^*}$], [$C_{ant}^{TTD}$]) within each box of the A05 section, for the period 1992-2011, where studied by two different approximations, as reported in section 3.3 and 3.4. The first one consisted in performing linear regressions between the five years in which the different datasets were obtained and their corresponding [$C_{ant}$] to estimate the respective decadal trend (DT, in $\mu mol \cdot kg^{-1} \cdot yr^{-1}$). The second approach consisted in the estimation of the respective $C_{ant}$ storage rates ($\mu mol \cdot kg^{-1} \cdot yr^{-1}$) assuming a steady state of the oceanic $C_{ant}$ distribution, considering a specific annual percentage rate of [$C_{ant}$] according to the literature. The following table summarizes the obtained results.

**Supplementary Table C1.** Decadal Trend (DT) ($\mu mol \cdot kg^{-1} \cdot yr^{-1}$) and Transient Stationary State Rate (TSSR) ($\mu mol \cdot kg^{-1} \cdot yr^{-1}$) by using each $C_{ant}$ method ($\varphi C_T^0$, TrOCA, $\Delta C^*$and TTD), for each box of the A05 section. The weighted DT and the mean TSSR of the four methods are shown in bold. The averaged time-normalized estimates of [$C_{ant}$] ($C_{anth}^{2000}$, $\mu mol \cdot kg^{-1}$) are also shown in bold.

| Layer | Region | Decadal Trend (DT) | | | | | Transient Stationary State Rate (TSSR) | | | | | $C_{anth}^{2000}$ |
|---|---|---|---|---|---|---|---|---|---|---|---|---|
| | | $\varphi C_T^0$ | TrOCA | $\Delta C^*$ | TTD | Weighted | $\varphi C_T^0$ | TrOCA | $\Delta C^*$ | TTD | Mean | |
| **uNACW** | **Florida** | 1.08±0.09 | 1.28±0.09 | 1.30±0.18 | 0.71±0.13 | **0.98±0.12** | 0.89±0.04 | 0.75±0.04 | 0.82±0.05 | 0.82±0.04 | **0.82±0.09** | **48.5±4.8** |
| | **R1** | 0.96±0.05 | 1.14±0.04 | 1.17±0.08 | 0.60±0.07 | **0.87±0.06** | 0.86±0.03 | 0.72±0.03 | 0.77±0.03 | 0.90±0.04 | **0.81±0.08** | **47.7±4.7** |
| | **R2** | 0.99±0.04 | 1.09±0.03 | 1.21±0.06 | 0.71±0.06 | **0.94±0.05** | 0.87±0.03 | 0.75±0.03 | 0.81±0.03 | 0.90±0.04 | **0.83±0.07** | **48.9±4.0** |
| | **R3** | 1.00±0.06 | 0.90±0.06 | 1.06±0.16 | 0.80±0.12 | **0.91±0.09** | 0.92±0.04 | 0.84±0.03 | 0.89±0.04 | 0.92±0.06 | **0.89±0.06** | **52.5±3.3** |
| | **R4** | 0.99±0.10 | 0.99±0.10 | 0.99±0.19 | 1.01±0.35 | **1.00±0.18** | 0.96±0.04 | 0.91±0.04 | 0.95±0.05 | 0.89±0.06 | **0.93±0.06** | **54.9±3.0** |
| **lNACW** | **Florida** | 0.48±0.11 | 0.77±0.12 | 0.72±0.24 | 0.15±0.16 | **0.41±0.15** | 0.51±0.04 | 0.48±0.04 | 0.54±0.06 | 0.53±0.05 | **0.50±0.07** | **29.5±4.3** |
| | **R1** | 0.49±0.08 | 0.56±0.07 | 0.54±0.14 | 0.32±0.10 | **0.44±0.10** | 0.59±0.03 | 0.57±0.03 | 0.59±0.04 | 0.58±0.04 | **0.57±0.05** | **33.8±3.0** |
| | **R2** | 0.40±0.06 | 0.47±0.05 | 0.59±0.10 | 0.45±0.08 | **0.46±0.07** | 0.62±0.03 | 0.60±0.03 | 0.64±0.03 | 0.63±0.03 | **0.61±0.05** | **36.2±2.7** |
| | **R3** | 0.37±0.06 | 0.41±0.06 | 0.55±0.10 | 0.60±0.09 | **0.50±0.08** | 0.68±0.03 | 0.68±0.03 | 0.70±0.03 | 0.71±0.04 | **0.68±0.05** | **40.3±2.5** |
| | **R4** | 0.53±0.06 | 0.62±0.05 | 0.70±0.09 | 0.56±0.07 | **0.58±0.07** | 0.72±0.03 | 0.71±0.03 | 0.73±0.03 | 0.71±0.04 | **0.71±0.04** | **42.0±2.1** |

| | | | | | | | | | | | | |
|---|---|---|---|---|---|---|---|---|---|---|---|---|
| **AAIW** | **Florida** | 0.38±0.15 | 0.28±0.13 | 0.38±0.24 | 0.03±0.18 | **0.19±0.17** | 0.24±0.04 | 0.24±0.04 | 0.30±0.07 | 0.20±0.04 | **0.25±0.08** | **14.6±4.9** |
| | **R1** | 0.43±0.08 | 0.42±0.07 | 0.48±0.15 | 0.31±0.09 | **0.37±0.09** | 0.31±0.02 | 0.35±0.02 | 0.36±0.04 | 0.28±0.03 | **0.32±0.05** | **19.2±2.8** |
| | **R2** | 0.29±0.04 | 0.29±0.04 | 0.37±0.07 | 0.15±0.06 | **0.24±0.05** | 0.27±0.02 | 0.32±0.02 | 0.34±0.02 | 0.25±0.02 | **0.29±0.05** | **17.3±2.9** |
| | **R3** | 0.08±0.06 | 0.04±0.06 | 0.22±0.09 | 0.03±0.07 | **0.06±0.07** | 0.27±0.02 | 0.31±0.02 | 0.34±0.03 | 0.27±0.02 | **0.29±0.06** | **17.0±3.3** |
| | **R4** | 0.27±0.05 | 0.29±0.05 | 0.43±0.09 | 0.16±0.08 | **0.25±0.07** | 0.28±0.02 | 0.31±0.02 | 0.35±0.03 | 0.30±0.02 | **0.30±0.05** | **17.7±2.6** |
| **uNADW** | **R1** | 0.42±0.05 | 0.52±0.05 | 0.54±0.08 | 0.47±0.06 | **0.48±0.06** | 0.30±0.01 | 0.39±0.02 | 0.38±0.02 | 0.30±0.02 | **0.34±0.05** | **20.4±2.7** |
| | **R2** | 0.09±0.04 | 0.15±0.04 | 0.22±0.06 | 0.20±0.05 | **0.17±0.05** | 0.23±0.01 | 0.31±0.01 | 0.32±0.02 | 0.18±0.01 | **0.26±0.06** | **15.7±3.6** |
| | **R3** | 0.06±0.04 | 0.08±0.04 | 0.28±0.07 | 0.11±0.08 | **0.12±0.06** | 0.16±0.01 | 0.21±0.01 | 0.25±0.02 | 0.12±0.02 | **0.19±0.06** | **11.0±3.6** |
| | **R4** | 0.19±0.04 | 0.20±0.05 | 0.38±0.08 | 0.16±0.11 | **0.21±0.07** | 0.15±0.01 | 0.19±0.01 | 0.25±0.02 | 0.13±0.02 | **0.18±0.05** | **10.8±3.2** |
| **lNADW** | **R1** | 0.19±0.05 | 0.26±0.05 | 0.26±0.08 | 0.18±0.07 | **0.21±0.06** | 0.19±0.01 | 0.20±0.01 | 0.12±0.02 | 0.22±0.02 | **0.18±0.04** | **10.7±2.4** |
| | **R2** | -0.01±0.03 | 0.02±0.03 | 0.10±0.05 | 0.14±0.06 | **0.07±0.05** | 0.15±0.01 | 0.14±0.01 | 0.09±0.01 | 0.12±0.01 | **0.12±0.03** | **7.4±1.6** |
| | **R3** | -0.02±0.03 | -0.05±0.03 | 0.06±0.06 | 0.13±0.21 | **0.01±0.06** | 0.12±0.01 | 0.08±0.01 | 0.06±0.01 | 0.09±0.06 | **0.09±0.04** | **5.1±2.4** |
| | **R4** | 0.02±0.04 | 0.01±0.04 | 0.09±0.07 | -- | **0.03±0.05** | 0.12±0.01 | 0.07±0.01 | 0.06±0.02 | 0.08±0.06 | **0.08±0.03** | **4.9±2.0** |
| **AABW** | **R1** | 0.11±0.10 | 0.20±0.10 | 0.16±0.19 | 0.05±0.16 | **0.11±0.14** | 0.16±0.03 | 0.11±0.03 | 0.08±0.04 | 0.14±0.03 | **0.12±0.05** | **7.1±2.8** |
| | **R2** | -0.05±0.04 | -0.03±0.04 | -0.03±0.07 | 0.04±0.06 | **0.00±0.05** | 0.15±0.01 | 0.10±0.01 | 0.07±0.02 | 0.09±0.01 | **0.11±0.04** | **6.3±2.5** |